Impact of local cross-sectional area reduction by local barrage placement on estuarine hydro- and morphodynamics

Author:	D.J.K. Schuurman
Student number:	4135792
Date:	June 2020
Supervisors:	dr. M. van der Vegt [1]
	dr. J.R.F.W. Leuven [2,3]
	[1] Utrecht University, [2] Royal HaskoningDHV, [3] Wageningen University
Institute:	Department of Physical Geography, Faculty of Geosciences, Utrecht University

Utrecht University

Abstract

Estuaries are morphological dynamic features, positioned on the edge between river and sea. Their morphodynamic evolution is the result of continuous interaction between the available sediment and the nonlinear tidal propagation giving rise to residual sediment transport patterns. There is an increased need for renewable energy and tidal energy generation in estuaries might be a viable option. Investments in the tidal resource fall behind to solar and wind energy because full exploitation of the tidal resource is hindered by the limited amount of knowledge on impacts of tidal barrages on estuarine hydro- and morphodynamics. Estuarine hydro- and morphodynamics are coupled to estuarine ecology which is considered valuable and is therefore protected in many of the potential tidal energy extraction sites.

This study aims to investigate the impacts of a tidal barrage placement on estuarine hydro- and morphodynamics. To assess the impacts of this, a 2DH Delft3D idealized estuary model was used. A depth-averaged approach was used to reduce calculation time in the Delft3D flow module. The tidal barrages were modelled as a local width reduction in the estuary. Different barrage configurations (degree of width reduction and location) were used to assess the hydro- and morphodynamic responses of the estuary. Additional model runs were included with a fixed bottom layer in and around the barrage mouth, reducing the maximum (mouth) depth. Only tidal forcing (M2 with amplitude of 1.0m) was included in the model, in combination with a small river discharge from upstream. The morphology was modelled up to a period of 34 years. All estuary parameters were kept constant in the model runs. Only tidal barrage positions and relative barrage mouth widths were varied between model runs.

The most important hydrodynamic responses included a decrease in tidal prisms of up to 3% and consequent decreases in water levels in the estuary. This led to a compression of the intertidal zone of 7 centimeter locally. The hydrodynamic response was immediate and decreased over time as the morphodynamic response grew. The morphodynamic response was predominantly visible in the area near the modelled barrages, up to a few kilometers away. The most important morphodynamic response was the increase of the depth in the barrage mouth (up to 8 meters) and the channels around the mouth. In the model runs with limited maximum mouth depth, the hydrodynamic response did not decrease considerably over time as the morphology around the barrage was not able to adapt to the new situation by channel deepening.

The material eroded from the channels near the barrage was transported seaward and partly deposited in the intertidal zone (based on the offshore low- and high-water lines). This resulted in an increase in area in the intertidal zone and an increase in the Vs/Vc ratio (volume of intertidal storage/volume of channels at mean sea level). Combined with an observed decrease in the a/h ratio (tidal amplitude/channel depth) this led to the conclusion that the system became stronger ebb-dominated by the placement of a tidal barrage. Resulting in sediment starvation starting from the middle estuary.

Contents

List of figures

List of tables

1. Introduction

1.1 Background

One of the simplest definitions used for estuaries is: “a body of water that has an inflow of river water and an open connection to the ocean” (Leuven et al., 2016). Estuaries occur in many different forms, depending on their formation history, climate, and degree of human interference. Estuaries are morphologically dynamic because they are situated on the border of the land and sea (figure 1), which makes them prone to rapidly fluctuating environmental conditions, influenced by catchment and oceanic processes (Hume and Herdendorf, 1988). The seaward boundary of an estuary is referred to as the estuary mouth, and seaward from this point the water is no longer semi-enclosed by land. Whereas the landward boundary is formed by the transition into the tidal river (figure 1). At this transition the typically converging estuary becomes constant in width and the morpodynamics are dominated by unidirectional river flow. Several of these dynamic morphologic features of estuaries are represented in figure 1. In this thesis, the focus will be on the abiotic estuarine components that are directly affected by tidal flow, like channels, inlet, shoals, intertidal flats, and the tidal river (figure 1). In the results and discussion more attention will be paid to the division of the total intertidal area over the lower, middle and upper estuary.

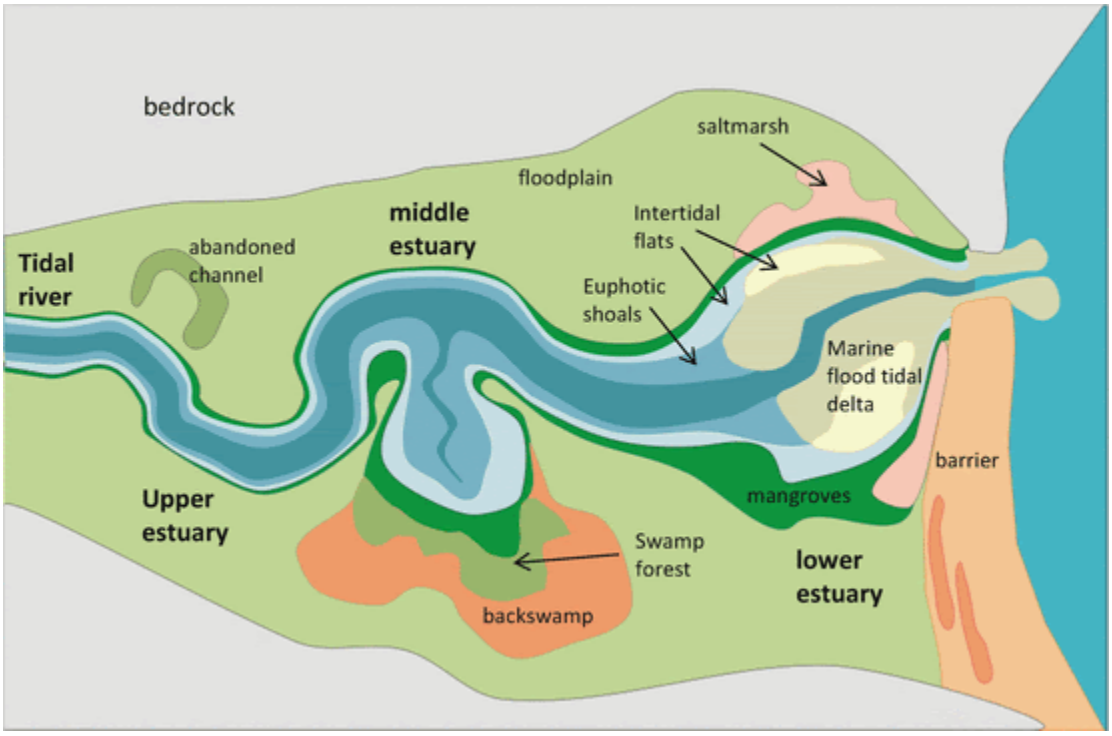

Figure 1, schematic representation with geographic and biologic nomenclature of estuarine components. Of importance to this thesis is the estuarine morphology, and so morphology of the tidal river and morphological features seaward of the mouth fall outside the scope of this thesis. Floodplains, saltmarshes, intertidal areas, and the marine flood tidal delta will be referred to as intertidal area for the remainder of this thesis as their elevation falls in the intertidal zone.

Many of the now existing estuaries are formed by the flooding of paleo river valleys as a result of postglacial sea-level rise during the Holocene (Dalrymple et al., 1992). The subsequent morphological development after the drowning of the river valley is a result of unidirectional river flow, bidirectional tidal flow, wave action and sea-level rise (Pye and Blott, 2014). The remnants of the drowned river valleys, that become the estuaries, and more specifically the mouth, can only remain open over multiple centuries to millennia when (1) the formation of accommodation space exceeds infilling or (2) the inlet system is in dynamic equilibrium (i.e., sediment input equals output) (De Haas et al., 2018). As a result of the formation by flooding of paleo river valleys and the subsequent hydrodynamic forming processes, most estuaries are characterized by a funnel-shaped outline (Savenije, 2015), widening towards the ocean. Because of the presence of side basins and curved outline (Nnafie et al., 2014) of the estuary basin, the funnel-shape can sometimes be hard to observe (figure 2, except for barrier).

There has been major interest in the development of tidal energy resource as a source of renewable energy over the past years (Cooper et al., 2009). Many of the studies, investigating the possibilities of the exploitation of the tidal energy resource have put estuaries forward as potential sites to do so (Burrows et al, 2009 II; Wolf et al., 2009; Pethick et al., 2009; Xia et al., 2010). The exploitation of the tidal energy resource in estuaries is done by making use of tidal barrages, like the one in the La Rance estuary (figure 2) (Retiere, 1994; De Laleu, 2009). The primary goal of such a barrage is to delay the flux of water to create sufficient hydrodynamic head between the external and internal water levels for energy generation, hereby hindering the natural hydro- and morphodynamics of the estuary (Burrows et al., 2009 I).

1.2 Problem description

The natural morphodynamic equilibrium state in an estuary, if even fully established, is a precarious state that can easily be disturbed by changes in a wide variety of natural processes, such as sediment supply, wave action, or tidal wave propagation (Dronkers, 1988). Placement of a tidal barrage within an estuary will affect all these natural processes, thereby bringing the system out of morphodynamic equilibrium. Other well-known examples of these man-made interventions that bring natural systems in disequilibrium are damming of rivers, deepening of channels to improve navigability, or reduction of surface area by closure of secondary basins employing hard coastal defense structures along their fringes (Ibàñez et al., 1996; Hibma et al., 2008; Van Maren, 2015; Nnafie et al., 2018).

Most of these (man-made) alterations to the dominant forming processes of estuaries are implemented for the sake of economics, to improve safety from floods, or in this case, (renewable) energy supply. These economic, flood safety and energy supply adaptations often have consequences for the hydrodynamics (faster propagation of tidal wave throughout basin and tidal amplification) (De Jonge et al., 2014), and all these adaptations and their consequences have an impact on the flora and fauna that live in the estuaries (Veríssimo, et al., 2012). The extent of salt marshes, mudflats, and sandflats (figure 1), which function as nursery or spawning grounds for fish and birds (Wolf et al., 2009), are a clear example of this and the growth or decline of their extent is directly influenced by altered hydrodynamics. These intertidal mudflats, sandflats, and salt marshes often accommodate unique flora and fauna and are therefore considered valuable (Wolf et al., 2009).

1.3 Knowledge gap

The placement of a tidal barrage in an estuary for the exploitation of the tidal energy resource will be the focus of this thesis. The placement of a tidal barrage will result in direct alteration of key forming, hydrodynamic constituents of a natural estuarine system. Essentially, a tidal barrage is a hard structure

built across a tidal basin or estuary to delay the flux of water to create sufficient water level difference for turbine operation (Burrows et al., 2009 I). The delay of water flux has consequences for the water levels in the estuary, as well as for the tidal prism. A tidal barrage usually consists of hard impenetrable parts, sluices and turbines/generators (figure 2) (Andre, 1978). The hard, impenetrable parts cause a local width reduction of the estuary and concentrate the water flow through the turbines/generators, altering the local hydro- and morphodynamics.

Several studies have been conducted to test the feasibility of large-scale systems to extract tidal energy from natural estuaries and their consequences for natural systems (Burrows et al., 2009 I; Burrows et al., 2009 II; Wolf et al., 2009, Pethick et al., 2009; Xia et al., 2010). Two (large-scale) tidal barrages have actually been implemented and are currently in operation, which is, next to the one in the Rance estuary in France (Retiere, 1994) (figure 2), the one in Lake Shiwa in South Korea (Young, Kyeong, and Byung, 2010). Both barrages have an energy output of around 500 kWh/year.

Examples of tidal basins or estuaries that have been studied for their suitability for the placement of a tidal barrage are the Grevelingen Meer (Turlings and Nieuwkamer, 2009; Wang, 2010), Severn estuary (Xia et al., 2010), and Mersey estuary (Burrows et al., 2009 II) (figure 3). For the Severn and Duddon estuaries, several locations were studied (Falconer et al., 2009; Cooper et al., 2009) based on the presence of natural headlands/islands or impacts. Although all of these studies have been conducted to test tidal barrage feasibility and two tidal barrages are currently in operation, the exact effects on estuarine morphodynamics of a newly implemented tidal barrage still remain vague. As the exact impacts of the exploitation of the tidal energy resource remain unclear, investments fall behind other renewable energy sources, like wind and solar energy (Neill et al., 2009).

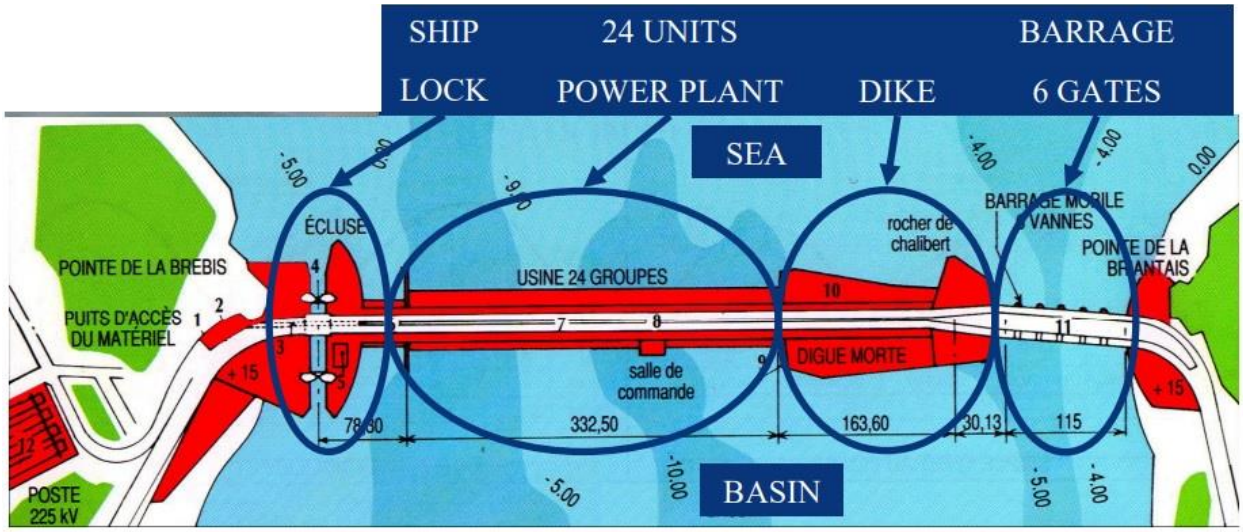

Figure 2, overview of La Rance tidal power plant, which is the 2nd largest working tidal range energy generation facility in the world (Andre, 1978). The barrage gates are used to create sufficient head between the estuary and open sea, after which the flow is directed through the turbines, hereby delaying and concentrating the flux of water. Distances in meter are indicated below barrage components. The barrage part is solely used for letting water into the basin.

1.4 Objectives

The objective is to study the effect of inlet width reduction, and thereby cross-sectional area reduction in an estuary, which could be expected as a result of tidal barrage implementation. The location of a tidal barrage is not necessarily restricted to the estuary mouth as headlands/islands or human-structures sometimes provide opportunities elsewhere (Falconer et al., 2009; Turlings and Nieuwkamer, 2009).

Therefore, 3 degrees of width reduction will be tested in combination with 3 different locations within a modelled estuary in Delft3D.

The effect on both the estuarine tidal hydrodynamics as well as on the consequent estuarine morphodynamics will be studied. Moreover, the degree of cross-sectional area reduction and position of the barrage within the basin is expected to strongly influence the hydro- and morphodynamic response of the system. The altered hydrodynamics will be observed over time and discussed. The same holds true for the morphodynamics which generally show alterations on a longer timescale.

This study could form an addition to earlier studies who were conducted by solely making use of existing literature and model data (Wang, 2010), only assessed the hydrodynamic effects of tidal barrage implementation (Xia et al., 2010), or solely based their research on empirical observations from the La Rance tidal barrage (Retiere, 1994). The most important findings of these studies include, the deepening of channels and relocation of channel networks and tidal flats close to the (possible) barrage (Wang, 2010; Retiere, 1994), erosion and decrease of intertidal area (Wang, 2010), and a decrease of high water levels and tidal prisms in the landward part of the estuary (Xia et al., 2010).

2. Literature review

This literature review will be used to provide better insights in the current knowledge in several fields of study, to hopefully improve the reader's understanding of the remainder of this thesis. In this literature review, first, a synthesis of the most important and relevant subjects/features of tidal energy generation will be provided. Secondly, a short synthesis of the most relevant literature on tidal wave distortion in estuaries is presented, and thirdly the relevant literature on estuarine morphology and tidal flats is summarized. From the additional information this literature review will provide, combined with the objectives that were set in the previous section, three research questions will follow at the end of this chapter.

2.1 Tidal Energy

2.1.1 Tidal energy extraction

Tidal energy could make a significant addition to the total of renewable energy sources. Especially in the UK, more precisely in the Severn estuary and the Irish Sea (figure 3). Here the tidal range energy has the potential to play an important role: 10% of the present total electrical energy demand should be attainable by using the tidal energy resource to its full potential (Burrows et al., 2009 I). A big advantage tidal energy has over other renewable energy sources, is that it is highly reliable and predictable (Burrows et al., 2009 II). However, investments fall behind to wind and solar energy because full exploitation of the tidal resource is hindered by the limited amount of knowledge on impacts (Neill et al., 2009).

It should be emphasized that the tidal resource can be exploited by making use of tidal barrages as well as free-standing tidal stream turbines. The energy generation by making use of tidal barrages is also referred to as tidal range energy (Burrows et al., 2009), whereas the energy generated by submerged stream turbines positioned in straits and on headlands is referred to as tidal stream energy (Neill et al., 2009; Stevens et al., 2012).

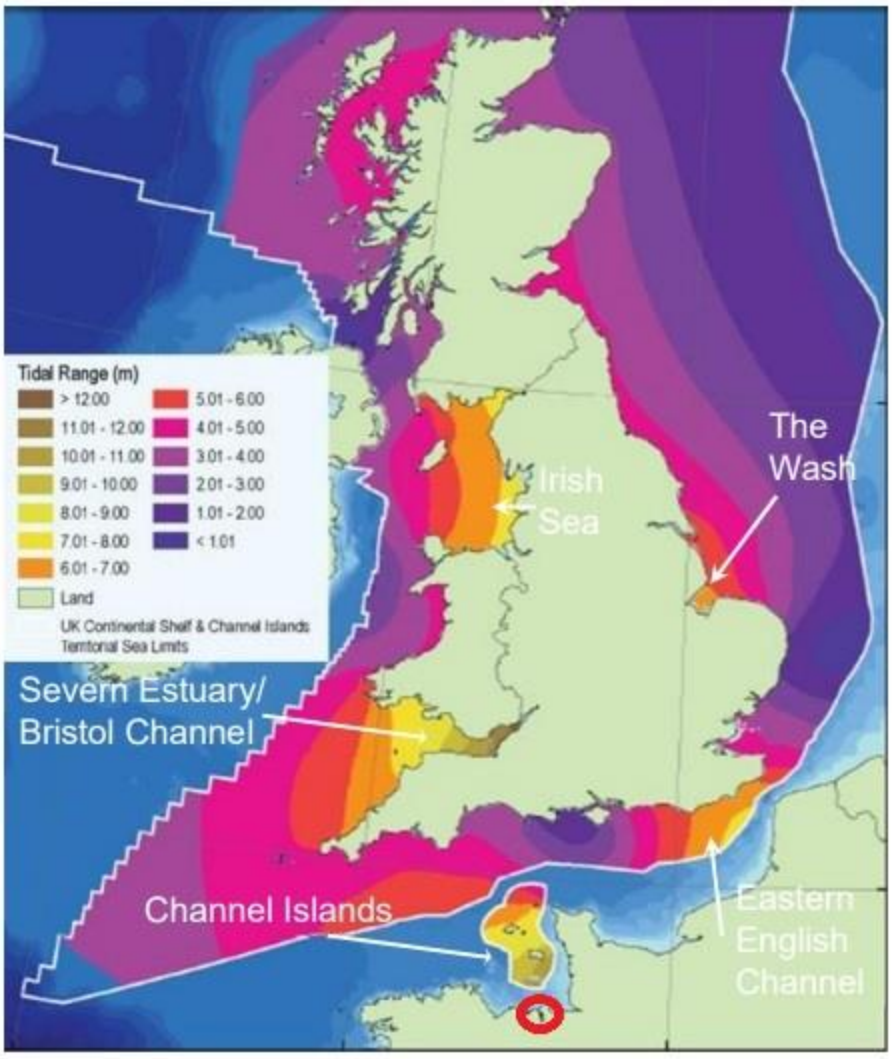

Figure 3, potential sites for the extraction of tidal range energy, investigated in various studies and mentioned in this literature review. The main factor that determines the suitability for generation of tidal range energy is the tidal range. The location of the La Rance tidal plant is indicated by the red circle in the Mont Saint-Michel Bay, south of the Channel Islands. The average tidal range at the Rance estuary is 8.2 meter (de Laleu, 2009. From: Cooper et al., 2009.

Many of the potential sites for the construction of tidal energy barrages are located within estuaries (Hooper and Austen, 2013). Tidal range is key parameter in the generation of tidal range energy (figure 3). High water levels are often increased in (strongly) converging estuaries by an effect that is called tidal wave amplification. This increases the tidal range in estuaries. The combination of tidal wave amplification with the constant input of river water make estuaries so suitable for tidal range energy extraction. In estuaries it is unlikely that tidal stream options can come close to the energy yield of barrage alternatives (Burrows et al., 2009 II). Although tidal lagoons are often considered as alternative locations for the generation of tidal range energy, it is highly unlikely that they could be realized on the same scale while remaining cost-competitive against estuarine tidal barrages (Burrows et al., 2009 II). This is mainly due to the length of barrage needed for the construction of tidal lagoon. Whereas in an estuary, a relatively short barrage would suffice to close off the system from the open sea. This is related to the fact that longer barrages are more costly to construct than shorter ones.

Tidal range energy can be generated within estuaries by the construction of a tidal barrage, which is a dam-like structure across an estuary to create a reservoir that can be closed off from external tides (figure 2). The primary goal of the barrage is to delay the flux of water as external tidal level changes, while the internal water levels are kept constant and supplemented by river water. The barrage does so to create sufficient head or water level difference for turbine operation (Burrows et al., 2009 II). For the remainder of this thesis, the focus will solely be on the generation of tidal range energy in estuaries by making use of a tidal barrage, the exploitation of the tidal resource by making use of stream turbines falls outside the scope of this thesis.

2.1.2 Tidal power schemes

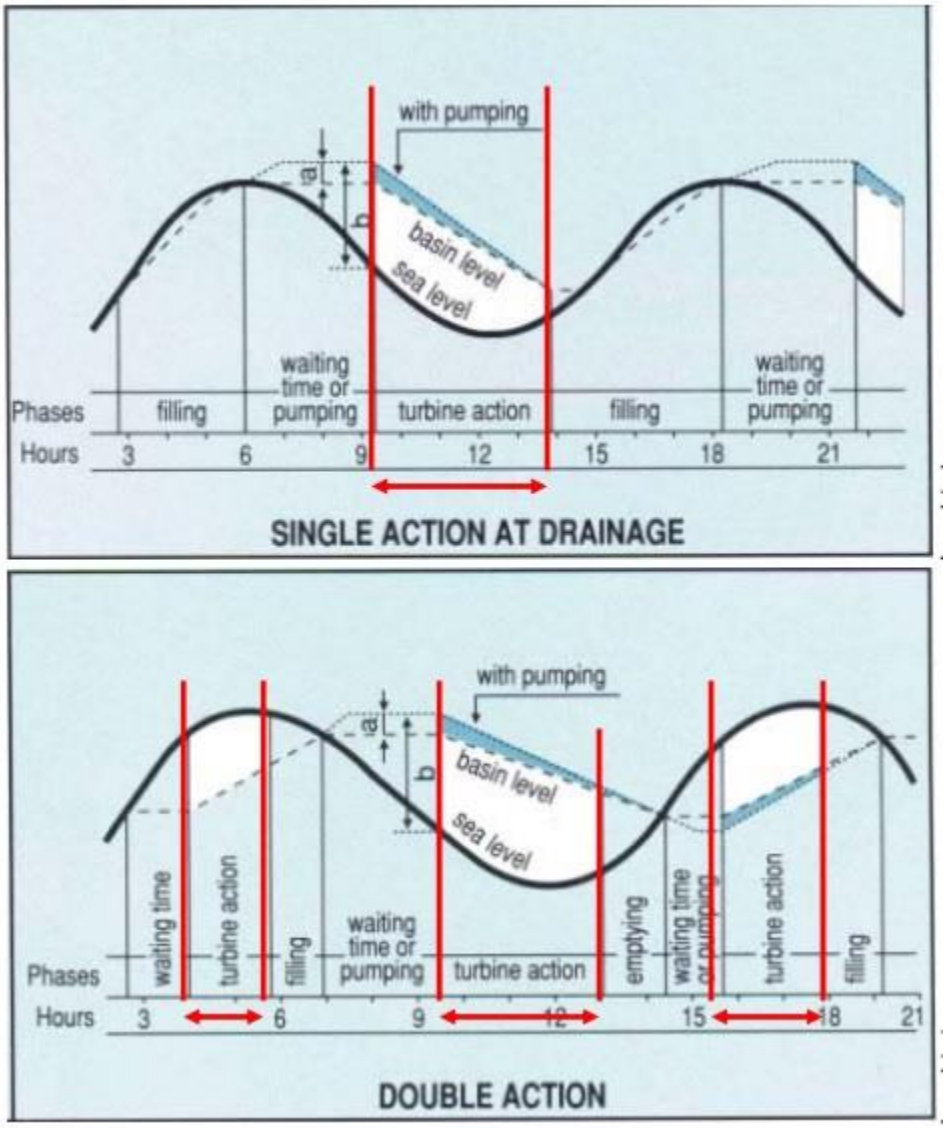

Figure 4, One (upper panel) and two-way generation. Summed length of red arrows, which is the time window of generation is larger in two-way generation, but effective yield is still smaller due to smaller head and turbine efficiency. From: de Laleu, 2009

An important aspect of the tidal power schemes is that, while extracted energy is proportional to the tidal amplitude squared, the requisite sluicing area is proportional to the square root of the tidal amplitude (Prandle, 1984). As a consequence, sites with large tidal range are most suitable for tidal generation (figure

3), while sites with small tidal ranges are limited by sluicing costs. An example of a site that might be well suited for tidal range energy generation is the Irish Sea (figure 3). Several studies have looked into the feasibility of tidal range energy extraction in the bays and estuaries around the Irish Sea, which could potentially account for half of the total regional energy demand (Burrows et al., 2009 I; Wolf et al., 2009).

The tidal power scheme is based on the minimal difference in elevation between the external tide and the water level inside the basin (b in figure 4). The minimal elevation difference determines the time range in which power generation is possible in both one-way/ebb, and two-way generation (figure 4) (Prandle, 1984). The minimal elevation difference is generally smaller in the two-way generation type of barrage and so the time window of generation is larger. Although the time window for generation is generally larger in two-way generation, the total yield is smaller, as one-way generation works with larger water elevation differences and two-way generation requires special turbines with smaller efficiency (de Laleu, 2009). The La Rance tidal power plant, which is one of the few tidal barrages being in operation, is considered a success and has been actively using both ebb-generation and two-way generation (Charlier, 2007).

2.1.3 Tidal barrage effects on estuarine hydro- and morphodynamics

An important hydrodynamic implication of placement of a tidal barrage in an estuary is that the tidal range inside the basin will decrease considerably (Wolf et al., 2009). This will directly affect other hydrodynamic parameters, like water levels and flow velocities (Cooper et al., 2009), in the basin. Because of this water quality and sediment regime are affected indirectly (Wolf et al., 2009). In general, the effects on the tidal range will be as follows: ebb-generation uplifts the low water levels, high water levels within the basin are reduced by flood generation, and two-way generation results in smaller amplitudes for both ebb and flood water levels (figure 5) (Burrows et al., 2009 I). A modelling study assessing the effects of tidal barrage implementation in the Severn estuary (figure 2) predicted maximum water level reductions of 0.50-1.50m and a maximum uplift of 5.00m of minimum water levels in the upper estuary (Xia et al., 2009). From a flood safety point of view the reduction of maximum water levels could be beneficial (Cooper et al., 2009). But the reduction tidal range would be harmful to ecologically important intertidal areas like saltmarshes (Wolf et al., 2009; Xia et al., 2009).

Next to tidal range also the position of the new mean water level inside the basin will be altered: because the minimal hydrodynamic head needs to be respected to generate power, the mean water level will be altered considerably, namely 10s of centimeters to meters (figure 5). In the La Rance estuary the new mean water level is 2.5 meters higher than it was prior to barrage construction (Retiere, 1994). The alteration of the mean water level for ebb generation also would negatively affect intertidal ecology because it would compress and shift the position of the intertidal zone (Gordon, 2008). On the other hand, the reduction of tidal currents in a highly dynamic estuary could decrease the suspended matter concentration in the water and increase the light penetration, resulting in potential higher benthic biodiversity and higher levels of aquatic life in the estuary (Falconer et al., 2009).

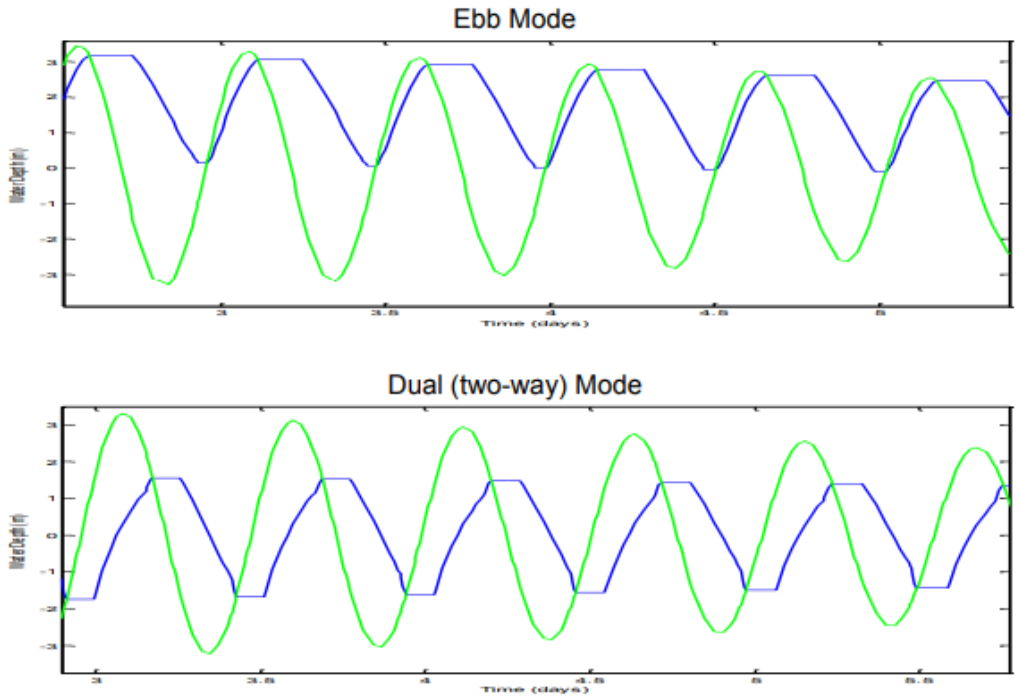

Figure 5, modelled Dee barrage (figure 4) water levels, using a 0D-model or "two-tank model" for different operating modes for spring tide phase based on M2 and S2 tidal constituents. External tide level in green and basin water level in blue (Burrows et al., 2009 II).

In general, the geomorphological impacts of barrage placement, especially in relation to impacts on salt marshes and mud flats, which will be referred to as intertidal area, are poorly understood (Cooper et al., 2009). The implementation of large-scale tidal barrage schemes in the UK is to a large extent hampered by ecological concerns, as most of the estuaries suitable for tidal range energy extraction are protected as part of the Natura 2000 program. The ecological consequences are closely tied to the hydrodynamic and morphodynamic ones. Ecological concerns include the expected loss of fish spawning grounds, loss of bird winter feeding grounds, and the lack of knowledge on the impact on invertebrate populations under reduced tidal influence (Cooper et al., 2009). In the Netherlands this is less of an issue as the re-opening of currently (semi) closed basins like the Grevelingen Lake or Haringvliet could even be beneficial for local ecology, but here the energy generation is not cost-effective due to smaller tidal ranges.

What is clear on the morphologic effects of tidal barrage implementation concerns the creation of areas of increased erosion of estuary bottom near the barrage. This leads to shifted sandbank positions, coarsening of the bed sediments, channel deepening around the tidal barrage. It was observed that this had consequences for local fauna in the La Rance estuary, like temporal decrease in invertebrate communities (Retiere, 1994). The loss of intertidal area, which includes salt marshes and mud flats, was also put forward as an important morphological effect by Wang (2010).

2.2 Estuarine hydrodynamics

2.2.1 Tidal forcing

As described in the previous section, possible tidal barrage implementation is expected to have profound effects on estuarine hydrodynamics. And in its turn, estuarine morphology, which is to a large extent determined by large-scale hydrodynamics and residual sediment transport patterns (Dronkers, 1986). Residual sediment transport patterns arise from a variety of factors, of which the most important for this thesis are: the distortion of the tidal wave propagating in the estuary, and the river input (Dronkers, 1986).

The tidal forcing is essentially caused by change in water level under the influence of the gravitational forces of Sun and the Moon. When plotted over the time, the water level fluctuations (of the separate tidal constituents) are expected to follow a perfect sinusoidal path (figure 6, solid line). This perfect sinusoidal behavior can hardly ever be observed in nature where the incoming tidal wave shape gets altered as a result of tidal wave distortion (figure 6, dotted line). The same holds true for flow velocities, plotted over time. The non-linear distortion of the tidal wave is composed of two factors: the frictional interaction between the tide and the bottom in the channels, and the intertidal storage (volume) (Friedrichs and Aubrey, 1988). It is expected that by the placement of a tidal barrage, the channels around the tidal barrage will deepen and the local intertidal storage will decrease. This will likely have an impact on the distortion of the tidal wave and the resulting sediment transport patterns.

Other factors that play a role in the pattern of the residual sediment transport are river inflow, sediment characteristics and wave action (Dronkers, 1986). These factors will be dealt with in more in detail in the methodology chapter.

2.2.2 Tidal wave distortion and overtides

Important features of the deformed tidal wave are the difference between maximum tidal currents during ebb phase and flood phase, and difference between slack water periods preceding ebb and flood (Dronkers, 1986). The tidal wave shape is changed from sinusoidal to asymmetric because of small mean water depths compared to tidal wave height and by changes in velocity field over a distance comparable to the tidal excursion as a result of channel geometry changes (Dronkers, 1986). The surface distortion or duration asymmetry grows with distance as the tidal wave propagates into the estuary. This distortion is a compromise between non-linear/depth-dependent frictional effects and intertidal water storage on tidal flats and in marshes (Friedrichs and Aubrey, 1988).

A measure to express the degree of tidal wave distortion is the ratio between the velocity or water level amplitudes of the first internally generated overtide: M4, and the incoming semi-diurnal tidal component: M2. Overtides are generated as a result of interaction between friction and the tidal wave and grow non-linearly in higher harmonics of the principal astronomical tidal components (Speer and Aubrey, 1985). The overtides of increasing order are generated in a cascade process with decreasing significance as their order increases (Lanzoni and Seminara, 1998). Because the semidiurnal lunar tidal constituent (M2) is the dominant tidal constituent in many regions on earth, the most significant generated overtide is the M2's first harmonic: the quarter diurnal lunar M4.

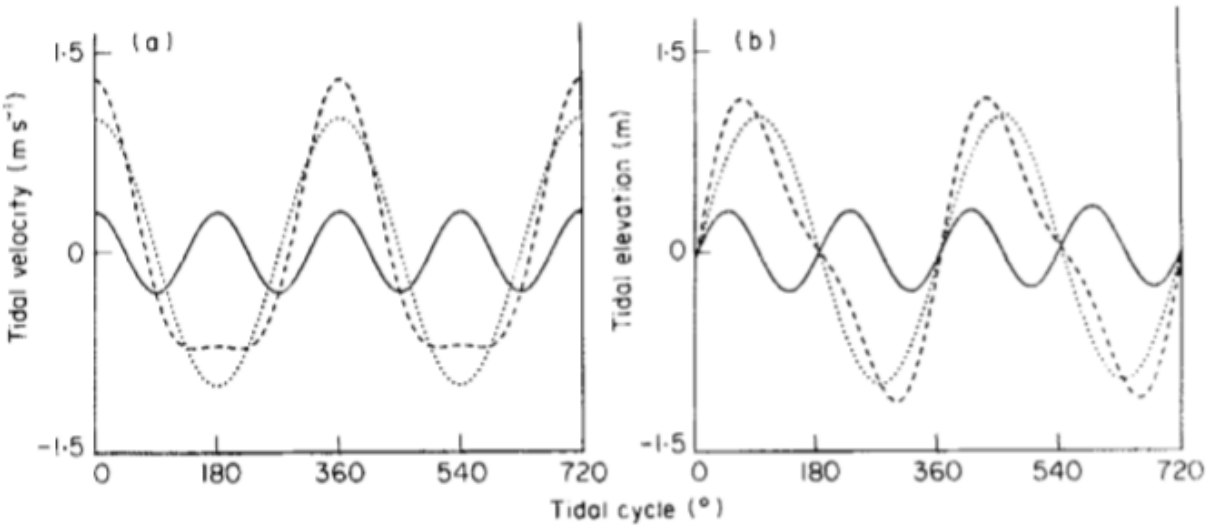

Figure 6, flood-dominance expressed in velocity amplitude (left) and ebb-dominance expressed in water level amplitude (right) asymmetry, from: Speer and Aubrey, 1988

2.2.3 Flood- and ebb-dominance

As a result of tidal wave distortion and tidal asymmetry, estuaries can become flood-dominant or ebb-dominant (Friedrichs and Aubrey, 1988). In flood-dominated systems, the degree of sea-surface distortion is controlled by the ratio between the offshore M2 amplitude (a) and average channel depth at mean sea level (h) and can be expressed by the ratio M4/M2. The a/h ratio is expected to increase in magnitude from lower estuary to upper estuary, as the mean channel depth decreases. In ebb-dominated systems the ratio Vs/Vc (storage of water over tidal flats/storage of water in channels) controls the sea-surface distortion (Friedrichs and Aubrey, 1988). Both the a/h ratio and Vs/Vc ratio, as well as the effect of the tidal barrage on these ratios, will be discussed in the results section.

From field measurements, it becomes clear that M4/M2 ratio does not exceed a value of 0.25 (Friedrichs and Aubrey, 1988). At this maximum tidal distortion, the asymmetry in landward sediment transport/seaward sediment transport (seaward sediment transport/landward sediment transport) can grow up to 1:2.25 (1:2.25) (figure 7). The M4/M2 ratio generally increases over distance from the lower estuary to the upper estuary. This is due to the internal generation of the first overtide M4 from the M2. The M4/M2 ratio is also influenced by the a/h and Vs/Vc ratios which reflect the estuaries geometry and therefore influence the tidal wave distortion. Where the M4/M2 ratio is a measure for the transport asymmetry, the nature and degree of transport is determined by the type of tidal wave distortion, which can be expressed as the relative phase difference between the M4 and M2 flow velocities. In the results section of the report it will be discussed how the placement of a tidal barrage influenced the nature and degree of sediment transport.

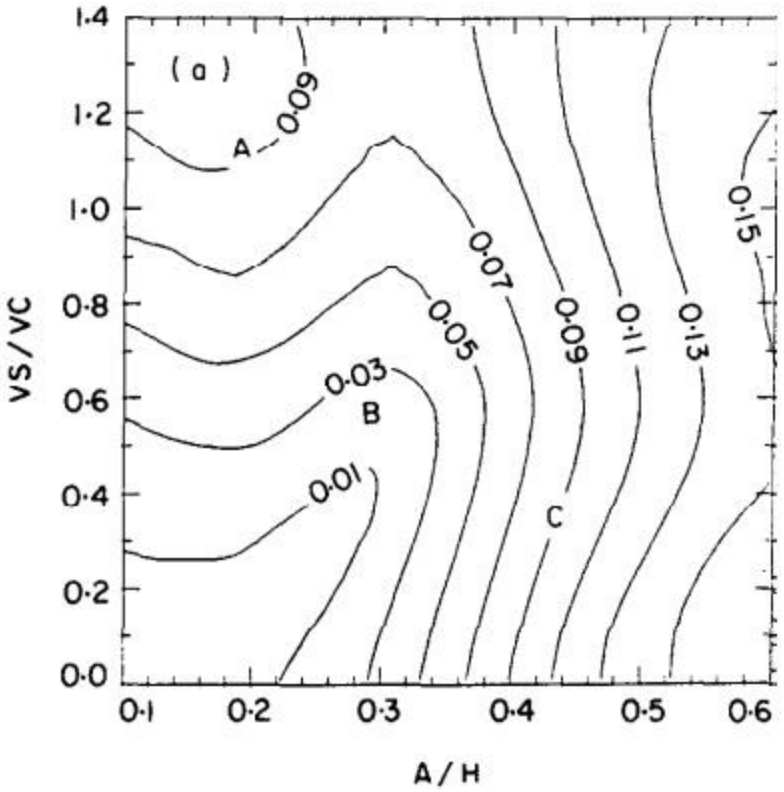

Figure 7, M4/M2 water level amplitude ratio contour lines, as a function of a/h and Vs/Vc ratio.The M4/M2 ratio is a measure for tidal wave distortion and can act as an indicator for transport asymmetry. The a/h ratio represents the offshore M2 water level amplitude divided by the local mean channel depth. Vs/Vc represents the ratio between water stored over the tidal flats and water stored in the channels. Ebb-dominant systems are characterized by low a/h ratios compared to Vs/Vc ratios. Flood-dominant systems are relatively deep and this is reflected by large a/h ratios to Vs/Vc ratios. From Friedrichs and Aubrey, 1988.

The nature of the transport asymmetry is determined by the estuarine morphology. A long-term change in estuary morphology is expected to be reflected directly by the a/h and Vs/Vc ratios, and over time also by the dominant sediment transport patterns. Duration asymmetry for example is caused relatively shallow channels, with large a/h ratios (range of natural a/h ratios depicted in figure 7). In these shallow channels, the (relative) depth (h) varies considerably over a tidal cycle, water depth is larger under the tidal wave crest than under the trough. This eventually results in relatively shorter floods and longer ebb periods because of depth-dependent friction (Dronkers, 1986). Because of this difference in duration between the flood and ebb period, the highest flow velocities are found during the flood phase. If a non-linear friction component (dependent on flow depth) is taken into account, the difference in propagation velocity between flood and ebb increases even further (Friedichs, 2010). The phase duration asymmetry leads to dominant landward transport of coarse sediment. For large a/h values, virtually all tested estuaries are flood dominant (Friedrichs and Aubrey, 1988).

Ebb-dominance, by contrast, is attributed to morphology dominated by relative deep channels and extensive intertidal water storage (Boon and Bryne, 1981). Ebb-dominated systems allow a relatively faster exchange of water through the deep channels around low tide than the slower exchange of water around high tide over shallow extensive tidal flats. This results in opposite duration asymmetry than in flood-dominant systems. The ebb-dominated systems are characterized by high values for Vs/Vc (figure 7)(storage of water over tidal flats/storage of water in channels) to a/h (offshore amplitude over channel depth) (Friedrichs and Aubrey, 1988).

Flood- or ebb-dominant systems, dominated by bedload sediment transport, with pronounced flood- or ebb dominant morphologies can only become more flood- or ebb-dominant, as flood dominant systems will only become shallower by sediment import and ebb-dominant systems grow deeper by exporting sediment (Friedrichs and Aubrey, 1988). The expected changes in water levels behind a newly placed tidal barrage might slightly influence the flood- or ebb-dominated character of the prevailing sediment transport patterns.

2.2.4 Wind and swell wave action

Wind and swell waves, also outside of storm events, are an important factor on which the large-scale sediment transport patterns in estuaries and tidal basins depend (Dronkers, 1986). The effect of waves is outside the scope of this project as the aim is to focus solely on the effect of the implementation of a tidal barrage on the estuarine morphology as a result of tide-induced hydrodynamics. According to Dronkers (1986), next to wave action, the evolution of an estuary essentially depends on two processes: the long-term averaged sediment supply and the abrupt changes in the morphology caused by storm surges or engineering works.

2.2.5 River influence

As described in the previous section, the long-term sediment supply is one of the two processes that are important in the evolution of an estuary. This sediment can be from inland or coastal origin. In the case of sediment with an inland origin, a river is a way to import this sediment from the catchment into an estuary. Next to that, river discharge can affect the water levels in the basin, the number of bars in along estuary direction, the braiding index and the bed level elevation (Bodewes, 2015).

2.3 Estuarine Morphodynamics

2.3.1 Estuarine classification

Part of this thesis is a morphodynamic analysis of an ideal funnel-shaped estuary is made. Therefore, a classification scheme based on the primary process that shapes the basin, combined with subsequent evolution by Holocene depositional processes, is presented in figure 8 (Hume and Herdendorf, 1988; Townend, 2005). The position of the funnel-shaped estuary in figure 8 will be used in the discussion chapter of this thesis.

Because various estuary types are considered to be representative of hydraulic processes, a morphometric classification scheme as provided by Hume and Herdendorf (1988) is used as a starting point. Special attention will be given to the cross-sectional area (CSA) at the estuary mouth, which will change considerably with the implementation of a tidal barrage and is considered a regulator of hydraulic processes (figure 9) (Dronkers, 1986; Townend, 2005). Normally the cross-sectional area of an estuary would be measured at the sea/estuary boundary. With the implementation of a tidal barrage, a locally narrower section is implemented somewhere else in the estuary. For analysis further in this thesis, the narrowest part of the estuary at the tidal barrage will be referred to as the mouth. And the cross-sectional area (CSA), which will be an important parameter for the remainder of this thesis, will be determined in this mouth.

The classification that Hume and Herdendorf (1988) present, many different subgroups based on the evolution of the basin. Most important for this thesis is the funnel-shaped estuary type. This is most important because it assumes a large inlet width with respect to mean width, tide-dominated

hydrodynamics, and extensive intertidal areas (numbers 1 and 4 in figure 8). The estuaries in the Irish Sea are predominantly of glacial origin, and later became drowned river valleys. They also inherited the typical funnel shape.

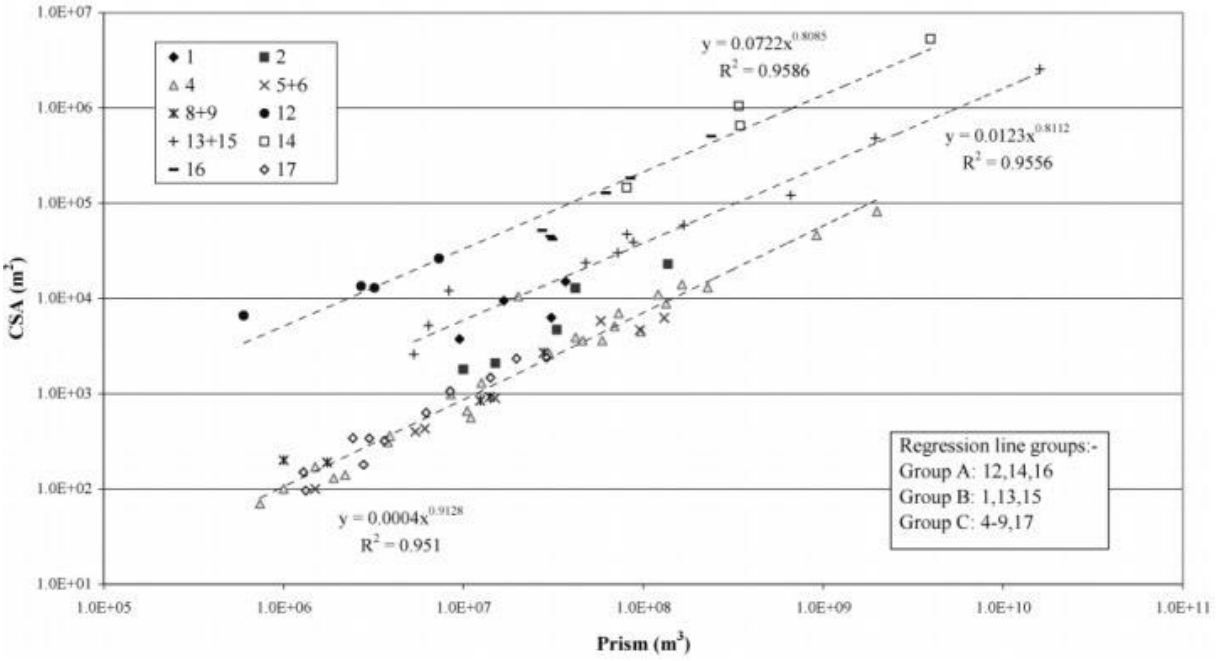

Figure 8, by Townend (2005); Cross-sectional area-tidal prism relation including the Hume and Herdendorf 1988 dataset. Trendline B and C, which are important for the remainder of this report represent elongated embayements and inlets/estuaries/rivers. Subgroup 2, in between dashed lines B and C, is also of special interest as it represents headland enclosed estuaries. Modelled cross-sectional area of the newly formed inlets in the tidal barrages and modelled local tidal prisms at barrages will be established at the barrages and compared to data in figure 8.

2.3.2 Empirical, morphologic relations: Cross-sectional inlet area-tidal prism relation

The initial classification by Hume and Herdendorf (1988) is included in the analysis by Townend (2005) and the analyzed basins are divided again, with the inclusion of their Holocene sedimentary evolution, into three groups: A, B and C (figure 8). In this classification by Townend, group A represents open embayments with resistant headlands that are generally wide and deep. Group B is composed of tidally controlled estuaries that are longer and narrower than the ones in group A and that form an intermediate endmember between more basin-like estuaries from group A and Holocene sedimentary processes-controlled endmembers from group C.

With the placement of a tidal barrage a local narrower section is introduced in the estuary. This narrower section could be considered to act as a new (headland enclosed) mouth. As originally, the estuary is expected to come from a morphodynamic equilibrium state, it could be expected that reducing the mouth CSA will trigger reactions that would restore the initial equilibrium state. A possible response of a narrower mouth would be to adapt by local deepening to accommodate the same tidal prism. Another response could be in the reduction of the tidal prism, as the flow of water through the narrower mouth is restricted. In general, the unlimited deepening of the estuary mouth at a tidal barrage is impossible as turbines positions and sluice bottoms are fixed by hard, concrete structures. To account for this, the maximum mouth depth is fixed in some of the model runs.

The empirical relation, presented in figure 8, will be used in order to check if the placement of a tidal barrage, hereby reducing the cross-sectional area (CSA) of the mouth, would considerably change the position of an estuary in figure 8. And so, if possibly the estuary would be classified differently, as for example, a headland enclosed estuary (group 2 in figure 8).

2.3.3 Empirical, morphologic relations: Bar dimensions-excess width

It is assumed that free-erodible bodies of water adjust themselves to external factors and dissipate free energy of these external drivers as efficiently as possible (Savenije, 2015). From this assumption, it follows that these systems must operate close to their hydrodynamic limits, which therefore would result in predictable patterns for several essential process parameters in estuaries, like estuary depth, water level amplitude and tidal width. The hydrodynamic limits also imply the funnel-shaped overall planform of estuaries as a result of decreasing tidal prism in the landward direction (figure 9) (Leuven et al., 2018a).

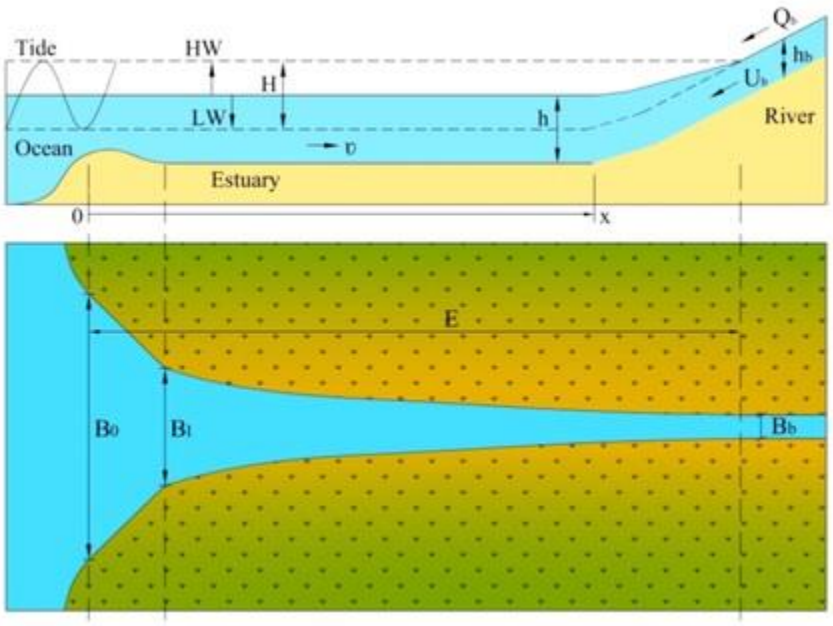

Figure 9, transect through an estuary (top panel) and ideal, funnel-shaped estuary planform (bottom panel). The estuary width (B), cross-sectional area (CSA) at every transect, tidal prism and depth all follow an exponential path in the ideal, funnel-shaped estuary. However, in natural systems the estuary planform always deviates from this ideal funnel shape.

However, many of the irregular alluvial estuarine planforms cannot simply be explained by the first-order relations as described by Savenije (2015) or covered by empirical relations like the ones presented by Townend (2005). That is partly because the estuary planform is not fully occupied by channels. The deviations from the ideal planform, as found in nature, can arise spontaneously, but the irregularities in are filled by bars (figure 10, top row) (Leuven et al., 2019). And so, the planform can seem very irregular, but the overall summed up channel width still follows the funnel-shape (figure 10). And the total local estuary planform width is filled by the total of the summed channel width combined with the summed bar width. This can be observed in the Western Scheldt, which has many partly closed, secondary basins (Nnafie et al.,2018) and therefore an irregular planform (figure 10, top left panel). However, the excess width that was left after the subtraction of the summed channel width by making use of an exponential fit, matches well to the measured summed width of bars in the estuary (figure 10, bottom left).

In estuaries, the location where bars form is determined by the channel excess width (Leuven et al., 2018a). The excess width is what remains after the summed width the channels, which obeys the funnel-

shape (figure 9), is subtracted from the total observed width of an estuary (figure 10, top row). The bar dimensions turn out to be directly coupled to the local excess width and local tidal prism. These parameters are linked to each other as discharge or local tidal prism (figure 10, middle row) determines the channel dimensions (figure 10, bottom) (Leuven et al., 2018a). This is where the outline shape of the estuary and the pattern and dimensions of bars come together. Because where local external restrictions limit the maximum width of the estuary a confluence of channels will develop as the excess width becomes negligible. At this point the brading index (which is the number of channels per estuary transect) is also expected to decrease to a value of 1, as no bars will be present within the confluence.

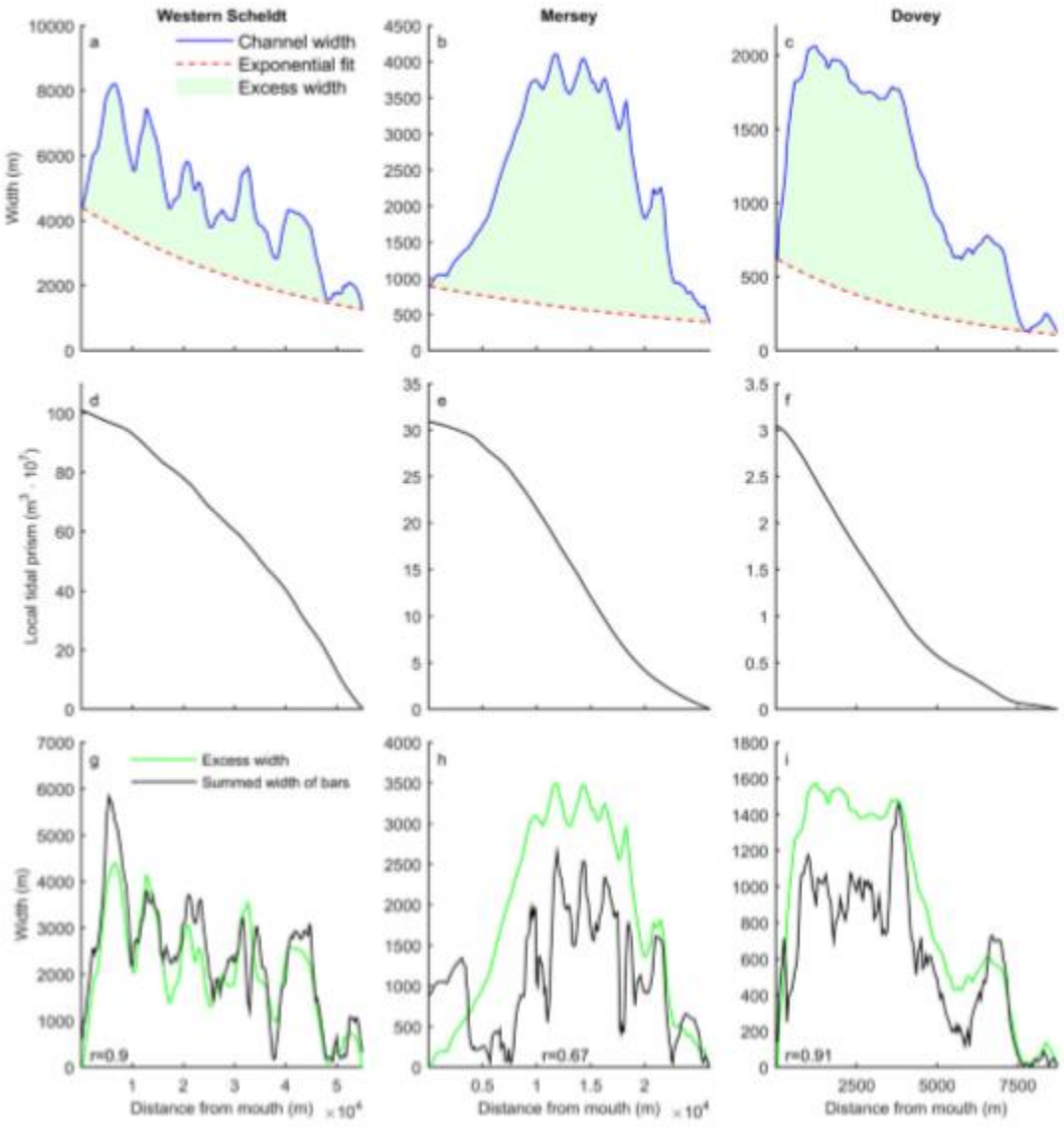

Figure 10, Channel width along estuary derived from planforms polygons for three estuaries (columns) with bathymetric data, by Leuven et al. (2018a). Representing excess width calculation based on exponential function fit to narrowest parts of basin (top), estimated local tidal prism (middle), and excess width – summed width of bar comparison (bottom).

This hold also true for the tidal barrage. At the tidal barrage mouth, the local channel depth will have to increase to accommodate the tidal prism as the estuary planform is restricted by the tidal barrage. Just landward and seaward of the tidal barrage, the planform restrictions are absent, but the channels are still

deeper than without the tidal barrage in place. So here extra excess width is present that could be filled up by bars. The sediment to make up these bars is comes from the deeper channels or is imported from somewhere else (Van Maanen et al., 2013). In the results a figure will be dedicated to the summed channel width around the tidal barrage.

2.3.4 Intertidal area: bars, floodplains, salt marshes

Bars, flats and marshes are distinct and ecologically important morphological features of the estuarine intertidal zone. So far throughout the introduction and literature review the terms intertidal area, tidal flats, and salt marshes have been used. As all of the terms refer to different features with different ways of formation, it is important for the remainder of this thesis to distinguish them from each other. For the remainder of this thesis everything in the intertidal zone will be referred to as intertidal area. The intertidal zone is defined as the zone in between the offshore low-water line (-1m) and high-water line (+1m).

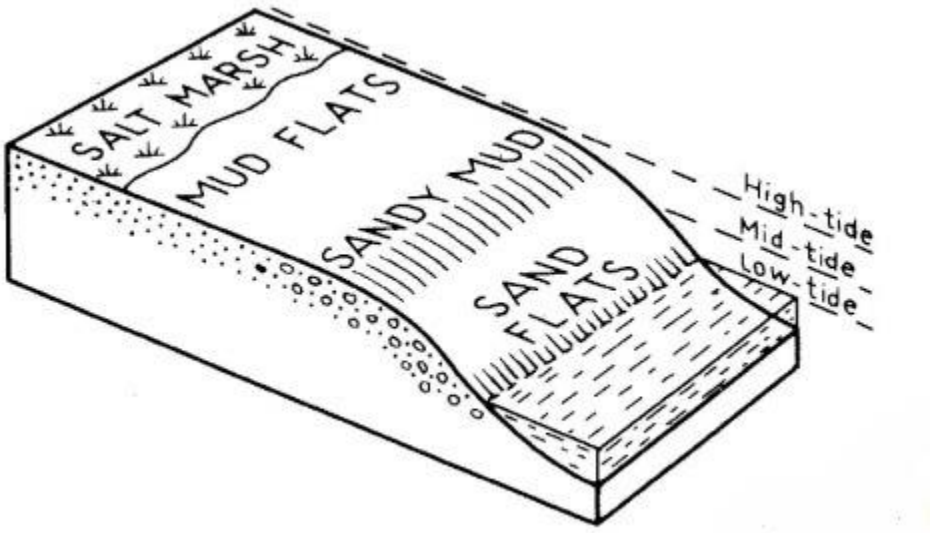

Figure 11, intertidal area subdivision. Different parts of the intertidal flats comprise different functions and ecologies.In the results section of this thesis, all of these parts are refered to as intertidal area, as there is no way to distinguish between them just on the base of elevation in the modelled estuary used. Source: Pethick, 1984.

Tidal flats are the low-relief, unlithified, regions between the high- and low-water line (figure 11). The intertidal flats generally catch sediment by tidal action, and are eroded by wave action (Friedrichs, 2011). Whenever there is a reference to intertidal area in the results section of this thesis, the definition for tidal flats also holds for the intertidal area. On the intertidal flats, mud is often present (Friedrichs, 2011). This mud moves to areas of least energetic conditions, which are present around the high-water line. Here vegetated and unvegetated mudflats can form, which both play important roles in ecology and are present in many of the earlier described Natura 2000 areas in the Irish Sea estuaries (Cooper et al., 2009). The vegetation on the mud flats can consist of salt marshes or mangrove forests. Closer to the creeks or channels, in higher energetic environments, sand flats can be found. They can be distinguished from one another by their composition.

In the previous section the term “bars” was frequently used. Bars form in the vicinity of channels and the rise of channels and subsequent bars is based on the conditions that cause instability in the uniform sloping estuary bed (Schuttelaars & De Swart, 1999). For the remainder of this thesis also bars will be classified as intertidal area for the same reason mud flats area.

Tidal flats provide storage space (Vs) and friction for the tidal wave (Leuven et al., 2019). This makes that they act as flood risk reducers. The total intertidal area and the division of intertidal area over the entire estuary will be discussed in the results section of this thesis. The connection to flood safety will return in the discussion section.

2.4 Research question

The research questions that follow from the knowledge gap, set objectives and literature review are the following:

1. What is the morphodynamic response of the estuarine morphology to local width reduction caused by, for example, tidal barrage implementation?
2. How is the morphodynamic response of the estuarine morphology influenced by the position of the local width reduction?

These questions will be answered by analyzing the most important hydrodynamic (tidal prisms, water levels) and morphodynamic parameters (channel depth, summed channel width, braiding index, CSA, intertidal area) and their response to the placement of a tidal barrage.

3. Methodology

3.1 General approach

This study aims to assess the effects of the implementation of a tidal barrage on the hydrodynamics, and consequently the morphologic evolution of an estuarine system. To be able to answer the research questions put forward in the first chapter, a Delft3D, 2DH hydro-/morphodynamic model was used.

To be able to find answers to the research questions involving the evolution of the hydrodynamics as well as the morphodynamics, the 2D hydrodynamics and morphodynamics needed to be solved. The Delft3D model used to do this, is only 2D because a depth-averaged approach was chosen to reduce the computational time (Bodewes, 2015). The data will be modelled in Delft3D flow module (Lesser et al., 2004) (figure 12) on a preexisting grid and depth profile that were provided by Bas Bodewes (section 3.3) *(*Bodewes, 2015).

3.2 Delft3D model

3.2.1 2DH hydro-/moprhodynamic Delft3D flow module

The system of equations used in the Delft3D flow module consists of the horizontal momentum equations, the continuity equation, and sediment transport (Lesser et al., 2004). The Delft3D flow module aims at predicting flow circumstances in shallow seas/estuaries/rivers in which horizontal length and timescale are significantly larger than the vertical scale (Lesser et al., 2004).

3.2.2 2DH Delft3D Oer-Ij estuary model

The Delft3D model of the estuary used in this thesis was initially built to assess the effects of river discharge, estuarine shape, and several modelling parameters on the estuarine bar pattern (Bodewes, 2015). The assessment of these effects shows strong similarities with the research questions as put forward in this thesis, except for the added local width/cross-sectional area reduction in the basin which will be described in more detail later in section 3.3.4. The Delft3D model set-up and grid were based on geologic reconstruction maps of the Oer-Ij estuary (Bodewes, 2015; Vos et al., 2010). The data that comes from the Delft3D flow module is later processed and analyzed by using Matlab. The figures containing Delft3D data therefore are also originating from Matlab.

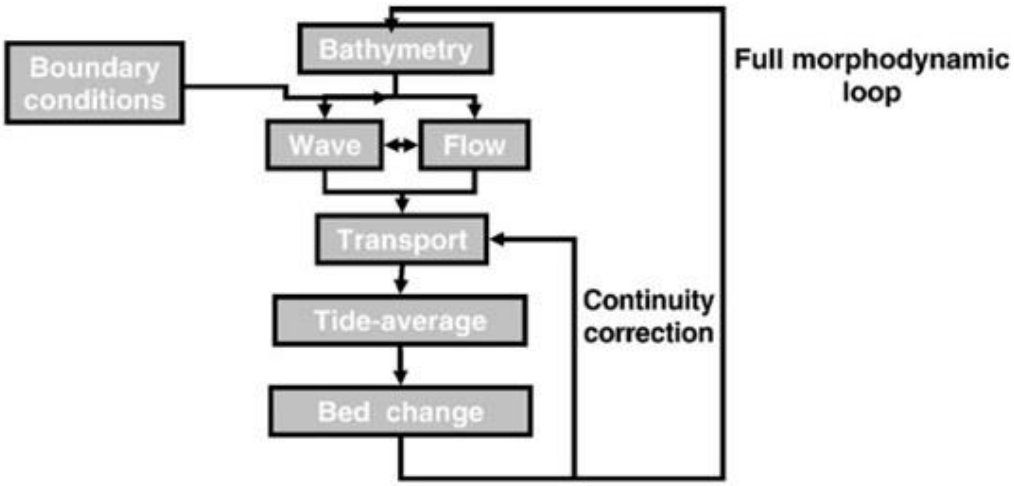

Figure 12, 2DH Delft3D feedback set-up as used for Delft3D flow module model runs in this report, from Roelvink and Walstra (2005). Every hydrodynamic timestep the morphology is updated, which in turn influences the hydrodynamics of system. The morfac (section 3.3.2) used in this thesis is 400. This implies that the morphodynamics works 400 times as quick as the hydrodynamics.

3.2.3 Estuary model domain, boundaries, and grid

In figure 13, the model domain and grid are presented. The model domain consists of a sea part, estuary part and a tidal river part. The estuary and tidal river part are symmetrical along the centerline to exclude possible effects of bends and side basins on morphologic evolution (Bodewes, 2015; Nnafie et al., 2018). For this thesis the straight version of the model provided by Bas Bodewes was used (Bodewes, 2015). This version of the model grid was used to be able to more easily assess the effect of the local width reductions.

The distance along the centerline of the estuary from the mouth to the end of the tidal river is about 45 kilometers in length. The estuary part itself is 28 kilometers in length along the centerline. The first 3 kilometers of the estuary from the mouth are constant in width. Just landward of this part, the width decreases over 25 kilometers from 3100 meter to 200 meters. The estuary is strongly convergent with a e-folding length scale of approximately 1/9 km (L_b^{-1}). The mean depth per transect of the initial bathymetry ranges from 4.3 meters near the mouth to 1.8 meter (figure 14, right panel) near the estuary-tidal river boundary.

Two closed and four open boundaries are present on the fringes of the model (figure 13). No flow can take place through the closed boundaries (Deltares, 2011, p. 207), which are positioned between the land and water parts of the model except for the river. To these boundaries a free slip condition applies, which implies that the effect of shear stress along these boundaries is neglected. One of the open boundaries is located on the right side of the model and represents the river boundary. The modelled tidal river has a constant width of 200 meters. For the model runs used in this report a constant discharge of 90 m^3/s was set at the river boundary and divided equally over the river width (Bodewes, 2015). No sediment influx was prescribed on the river boundary. This was done to observe more easily how the sediment would redistribute itself in the basin under the influence of the local width reduction. Wave action was also excluded from the model, to be able to better observe the effects of tidal barrage placement on the tidal forcing and how this affects the estuary.

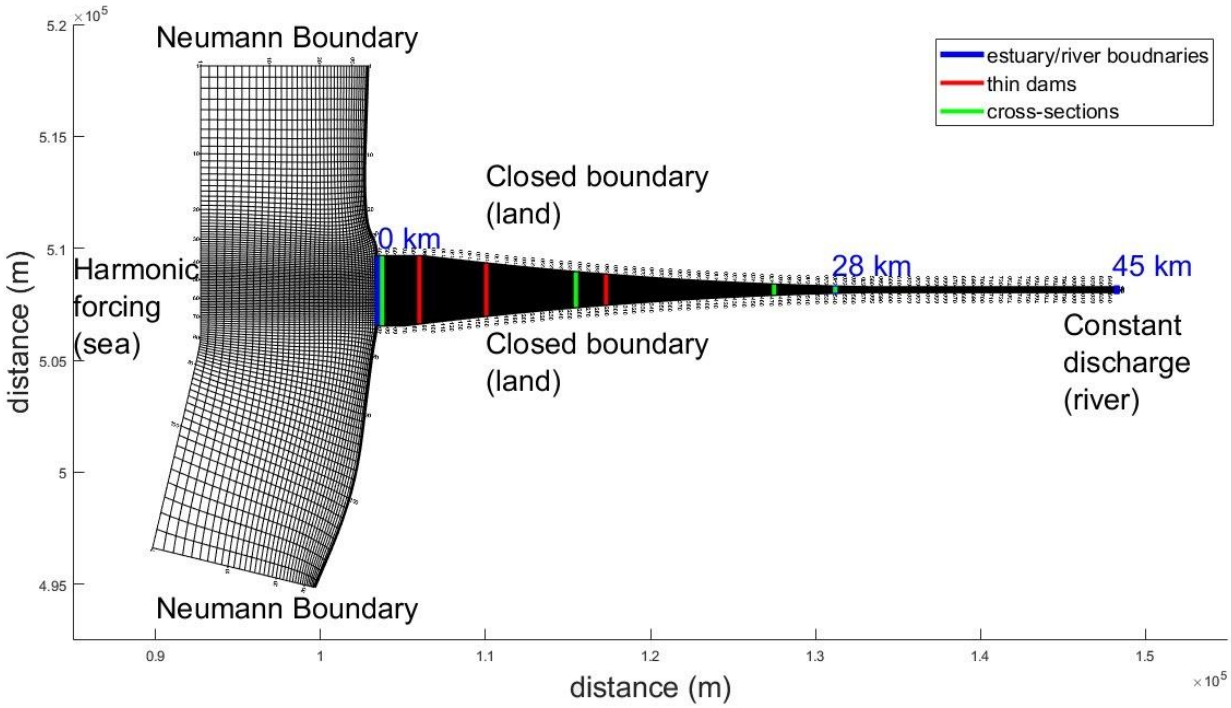

Figure 13, model domain and grid with distances measured along centerline from sea/estuary boundary in blue. Green transects indicate the positions of the hydrodynamic cross-sections and measurement points. Red transects indicate the three positions of the modelled tidal barrages. The Harmonic forcing and Neumann boundaries bordering the sea part of the model are open boundaries. The other boundaries are closed boundaries. At the tidal river boundary (right) a constant discharge of 90 m^3/s is set.

Along the left sea boundary, a constant water level amplitude is prescribed with a phase difference based on the boundary length (20 km), propagation speed of the wave and frequency of each of the tidal constituents (Bodewes, 2015; not table 1). In table 1 an overview of the combination of tidal constituents used in the data generation for this thesis is provided.

For all the runs, an M2 of 1.0 meter was prescribed at the harmonic forcing boundary (left). To be able to more easily study the distortion of the tidal wave, the first overtide (M4) is only internally generated. Only the initial amplitude of the O1 and M4 constituents were reduced to zero, but the constituents were not completely excluded, as the model was constructed and validated using these three tidal constituents (Bodewes, 2015). The values for begin phase were chosen in order to make sure that after the modelling period, all three constituents would be in equilibrium (amplitude=0) (Bodewes, 2015). The shape of the modelled shoreline led to alongshore propagating component of the tide. The alongshore component caused a slight asymmetry in the final morphology observed, but the exact role of the alongshore component of the tide lies outside the scope of this thesis.

Constituent	Frequency (°/hour)	Amplitude begin (m)	Phase begin (°)	Amplitude end (m)	Phase end (°)
O1	13.9438	0.00	7.4023	0.00	0.0000
M2	29.0323	1.00	15.4123	1.00	0.0000
M4	58.0645	0.00	30.8246	0.00	0.0000

Table 1, tidal constituents used in different runs and for the generation of the initial bathymetry (section 3.2.4).

The top and bottom model boundaries (figure 13) at sea are made up of so-called Neumann boundaries (Deltares, 2011, pp. 204-206). Both boundaries measure 10 kilometers in length. The Neumann boundaries, instead of using a fixed water level or velocity, allow the model to determine the correct propagation of the tide at these boundaries by imposing the alongshore water level gradient (Roelvink and Walstra, 2005). This is done to prevent boundary disturbances from occurring and to match the cross-shore water level and velocity distributions. Although the left (sea) and right (river) boundaries are "open boundaries", the reflection parameter (Alfa) used is 0, which makes these boundaries fully reflective (Deltares, 2011, pp. 49-52). The Neumann boundaries are open as well but not reflective.

A curvilinear grid was used, meaning that grid cell size is not constant (figure 13). The number of grid cells per transect within the estuary and the tidal river remains constant (n=36), but the grid cells become increasingly elongated in the landward direction, while the grid cell length in the estuary and the tidal river remains relatively constant around 50 meters. After generation of the grid in Delft3D RGFGRID, the grid was slightly orthogonalized in standard settings to optimize continuous flow. Grid boundaries were slightly altered to decrease sharp corners and subsequent disproportional erosion hotspots (Bodewes, 2015).

3.2.4 Bathymetry

The process of generating the initial equilibrium bathymetry is based on Bodewes (2015). Based on his work, a rectangular flat bed with width-averaged depth profile that was close to the final bathymetry of several of the conducted test-runs, was chosen as a starting point. The initial bathymetry used in the Delft3D model for this thesis was generated by running the model with the pre-initial bathymetry (provided by Bodewes) in combination with the set of harmonic components (table 1) for a period of 369 hydrodynamic days, which is equal to 403 morphodynamic years. This period was chosen because it was used in the generation of other equilibrium bathymetries in the work of Bodewes. And because after this duration no large-scale morphological changes were observed (Bodewes, 2015). The non-matching hydrodynamic and morphodynamic modelled periods can be explained by the inclusion of a Morfac value (Morfac=400) in the model. This essentially means that the morphodynamic evolution is sped up by a factor 400 with respect to hydrodynamic evolution. More on morfac in section 3.3.2.

3.2.5 Modelling period

For all model run incorporated in this thesis, the Ndep2 (figure 14, left panel) initial bathymetry was used. Results were gathered by running all models for the same amount of time, which is 31 hydrodynamic days or close to 34 morphologic years, as the Morfac used in all runs was 400 (more on Morface in section 3.3.2). The number of 34 morphologic years was established by the limited time available for doing all the runs and a realistic timescale over which tidal barrage effects should be tested and are comparable to the current timespan of the La Rance tidal power plant has been in operation.

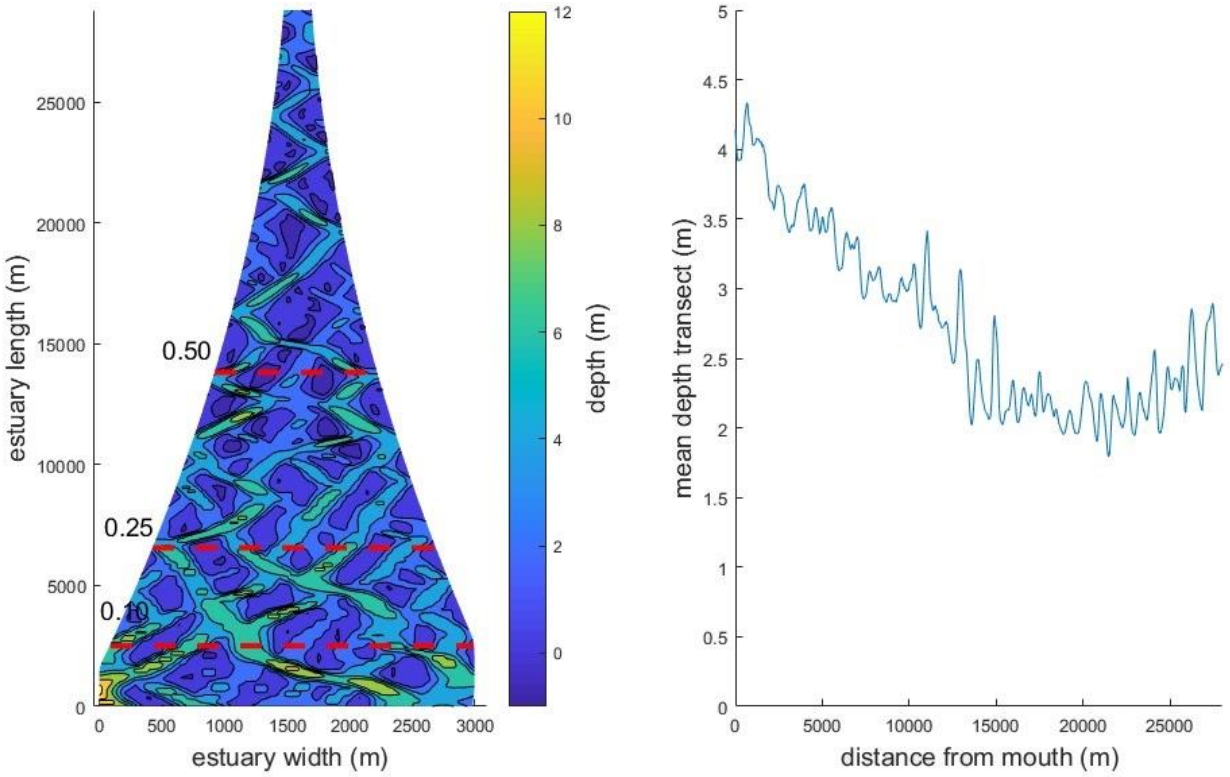

Figure 14, initial bathymetry (Ndep2) used in all conducted model runs of the converging estuarine part of the model only (left panel). Red, dashed lines indicate positions of tested thin dams at positions at relative locations 0.10, 0.25 and 0.50 of the total (converging) estuary length. A larger version of the equilibrium bathymetry, including more detailed is depicted in Appendix D. Morphology is compressed in the vertical direction for the sake of readability, so no conclusions should be drawn from bar pattern (shape). Right panel depicts the mean depth per transect of the equilibrium bathymetry for the entire estuary length.

3.2.6 Thin dams

To study the effect of the degree and position of the local width reduction on the estuarine morphology, three positions in the estuary model were chosen to include thin dams in the model (Deltares, 2011, pp. 418-419). For the remainder of this thesis, the thin dams in the model will be referred to as modelled tidal barrages or local width reductions. In Delft3D thin dams are infinitely thin objects which inhibit the flow between two adjacent cells. They essentially stop the exchange of flow through them but do not split the bathymetry. So, the bathymetry point that is positioned exactly underneath/within the thin dam will be used as depth in the calculations for cells on both sides of the thin dam (Deltares, 2011, pp. 36-38).

The tested locations of the thin dams were based on the total length of the converging estuary plus the approximately 3-kilometer-long straight part in between the sea and converging estuary part. The three tested locations are at the grid cells closest to $^{1}/_{10}$, ¼, and ½ of the length of the estuary from the mouth (including the constant width part). Next to the locations, also different local width reduction caused by the thin dams were varried. The total basin width reduction (per transect) at the locations of the tested thin dams is 75%, 50%, or 25% (table 3). For the most extreme width reductions of 75% also the maximum depth in and around the barrage mouth was limited for all tested locations. The maximum depth was fixed by reducing the total sediment bed thickness at these locations and was done to prevent extreme deepening of the mouth area. More on these limited depth runs (LD) can be found in the model run section (3.4). The locations of the thin dams within the modelled estuary are indicated by the red dashed lines in figure 14 and all the other figures for which the thin dam locations were considered relevant.

3.2.7 Cross-sections and hydrodynamic measurement points

At certain locations in the modelled estuary, measurement cross-sections and hydrodynamic measurement points were included. These cross-sections and measurement points were used to check the hydrodynamic parameters at these locations. They were located at 0, 15, 21, and 28 km from the sea/estuary boundary. Locations for the cross-sections match the locations of the hydrodynamic measurement points. Hydrodynamic data, like tidal prisms and water levels will be used in the results and discussion sections of this report. An overview of where the cross-sections and hydrodynamic measurement points are located, can be found in figure 13 (green lines).

3.3 Other parameters

3.3.1 Sediment and bed thickness

The sediment used in the 2HD Delft3D estuary model is non-cohesive fine sand with a grainsize of 200 µm. No silt or mud was used in any of the model runs to exclude the effect of cohesive sediments. In general, for the model runs a uniform 30-meter-thick sediment bed was used, that was never locally, completely eroded. Exceptions on this are the runs with limited maximum depth in and around the modelled tidal barrages mouth (LD-runs). For these runs the maximum thickness of the erodible sand bed was set at such a thickness that the total depth below mean sea level could never become more than 7 (or 8) meter, depending on the location of the thin dam and the initial bathymetry (table 3).

An important parameter that is connected to the sediment used is the transverse bed slope predictor. The transverse bed slope predictor affects not necessarily the magnitude of sediment transport but more the direction. This influences the location of sediment deposition hereby influencing the channel depth and bar length (Baar, et al., 2018). When both the Van Rijn (Van Rijn, 1993) and Engelund-Hansen sediment predictor (Engelund and Hansen, 1967) were tested, in the estuary Delft3D model used in this thesis, it turned out that the Van Rijn sediment predictor generated channels with transverse gradients that were out of order with the angle of repose for the non-cohesive sediment used. As a result, unrealistic deep and narrow channels could form (Bodewes, 2015). Although the Van Rijn sediment predictor is better able to model the transverse bed slope effect, the Engelund-Hansen predictor turns out to give better results for large-scale morphology in Delft3D (Baar et al., 2018). Therefore, the Engelund-Hansen sediment predictor is favored here over the Van Rijn sediment predictor.

3.3.2 Morfac

A way to bridge the gap between the short-term hydrodynamics and transport processes in Delft3D is the Morfac. The short-term (alterations in) hydrodynamics, represented by the tidal forcing takes place within days. The large-scale morphological changes, on the other hand, take periods of years to evolve. To overcome this difference in timescale, the morphodynamic acceleration factor (Morfac) is used (Roelvink and Walstra, 2005). Figure 12 represents a tide-averaged flow diagram in which the Morfac parameter would be used to match the short-term processes to long-term morphologic evolution. Tide-averaged (figure 13) indicates that the bottom is considered fixed during a hydrodynamic cycle because morphologic changes on these timescales are not expected to considerably affect the hydrodynamics (Roelvink and Walstra, 2005). In essence, the morfac parameter speeds up the morphological evolution to hydrodynamics because these processes take place on different timescales. The Morfac value used in the model runs included in this thesis is 400.

3.3.3 Other important parameters

Other important parameters that are excluded from this methodology section but that do play an important role in the Delft3D model, like Alfabn, Ashld, Chézy bed roughness and more, are still incorporated in the model but not altered from their initial state. A table including these parameters and their values used is incorporated in Appendix F. For more information and explanation of the parameters and parameter values used, see (Bodewes, 2015; Deltares, 2011).

3.4 Model runs

As the Delft3D model takes a few days (real-time) to complete a run, the number Delft3D model runs is limited. Much Delft3D hydro- and morphodynamic output was created in an attempt to find the right combination of parameter settings. The most important parameter settings and a more complete list of the Delft3D model runs conducted, can be found in Appendix B. During the process of finding the correct parameter settings, slowly a combination of parameter values was found and kept constant. This was done to be able to focus solely on the parameters and responses of the modelled system, related to the research questions. The 9 most important runs in which only the degree of local width reduction in the barrage mouth and position within the basin of modelled tidal barrage were varied, are presented in table 2. Cls_0_0_Ndep2 is the control case, which runs with the same settings but without a cross-sectional area reduction/modelled tidal barrage. The control run will often be referred to as "Cls-0-0".

Run Name	Width reduction (%)	Position TD	Max mouth depth (m)	LD layer length (m)
Cls_0_0_Ndep2	-	-	-	-
Cls_75_50	75	N=290	unlimited	-
Cls_50_50	50	N=290	unlimited	-
Cls_25_50	25	N=290	unlimited	-
Cls_75_25	75	N=160	unlimited	-
Cls_50_25	50	N=160	unlimited	-
Cls_25_25	25	N=160	unlimited	-
Cls_75_10	75	N=86	unlimited	-
Cls_50_10	50	N=86	unlimited	-
Cls_25_10	25	N=86	unlimited	-
Cls_75_50_LD(1)	75	N=290	7	171
Cls_75_25_LD(1)	75	N=160	7	171
Cls_75_10_LD(1)	75	N=86	8	171

Table 2, Delft3D model runs of which results are incorporated in report. N indicates the position of the modelled local width reduction within the modelled grid (figure 13). Cls_0_0_Ndep2 is the control run without width reductions and will often be abbreviated to Cls_0_0 or Cls-0-0 in figures. The first number within the Cls_.._.. code, indicates the percentage of local width reduction, the second number indicates the relative position within the (converging part of the) estuary. LD is an abbreviation for limited depth and the numbers in between the brackets () correspond to different lengths of non-erodible layers around the thin dam in the model runs. More info will be provided in the results chapter of this report.

All the 15 runs incorporated in table 2 will somehow contribute to the figures or data presented in the remainder of this thesis. In the process of presenting the data in combination with model run codes (Cls-..-..) it became clear that system chosen was too complicated. To overcome this problem, the number of data runs used in the results section was reduced as much as possible. After reduction of the number of runs presented in the results section, only 4 remained. These 4 runs are presented with their relative local width reduction (WR) and relative location (figure 14) in the estuary in table 3. The colors in which they are presented in table 3 will remain constant throughout this thesis.

The green run (Cls-75-25-LD(1)) requires some additional explanation. This run, although it uses the same tidal barrage settings as the purple run (Cls-75-25) is different from the other runs. The green run is one of the LD-runs, indicating that this has limited maximum depth in and around the inlet. The maximum depth in and around the modelled barrage mouth in the green run is 7 meters. The maximum depth was restricted to prevent deepening of the mouth, as found in the result of other model runs. Tidal barrages like the La Rance power plant always limit the maximum depth in and around the barrage mouth (De Laleu, 2009). Locally the maximum depth in this run was reduced by locally elevating the closed model boundary at the bottom of the estuary from 30 meters to 7 meters below mean sea level.

-	WR=0.75	WR=0.50	WR=0.25
Location=0.10	Cls-75-10	Cls-50-10	Cls-25-10
Location=0.25	Cls-75-25 / Cls-75-25-LD(1)	Cls-50-25	Cls-25-25
Location=0.50	Cls-75-50	Cls-50-50	Cls-25-50

Table 3, Overview of 4 most important Delft3D runs. WR indicates the degree of local width reduction, whereas the location indicates the relative location of the local width reduction from the sea-estuary boundary to the estuary-tidal river boundary. The codes, as depicted in this table will be used frequently throughout the remainder of this thesis.

3.5 Data reduction

All the data presented in the results chapter of this thesis (chapter 4) is directly originating from the Delft3D model runs. Hydrodynamic data (section 4.2) was generated in Delft3D and stored in trih-files. All the data presented in this thesis is directly originating from water levels, the cumulative discharge through the cross-sections, and cumulative sediment transport through cross-sections data stored in the trih-files. The same holds true for the morphodynamic data. This data is stored in Delft3D trim-files. All morphodynamic data presented in the results section is directly linked to the depth or DPS data stored in the Delft3D trim-files.

Braiding index (section 4.1.2), summed channel width (4.1.3) and area within the intertdal zone (4.3.2) analyses are based on manually grouping depth data in channels (below the offshore low water line of -1m) and area within the intertidal zone (above the offshore low water line of 1m). The braiding index was manually determined by counting the number of channels within a transect separated by intertidal area. For the sake of consistency the offshore low water line was used in the analyses and its positions was assumed constant over distance and time in every run.

4. Results

All the results focus on the hydro- and morphodynamic evolution of the estuary with a tidal barrage in place and how the estuary differentiates in its evolution from a situation without tidal barrages (Cls-0-0). To gain insights into the evolution process, the different hydro- and morphodynamic features are sometimes depicted over time, and sometimes as differential plots. The differential plots are meant to show the part of the estuarine evolution that is divergent from the estuarine evolution without tidal barrage in place. As described in the methodology section, the 4 runs presented in table 3 and the Cls-0-0 (control run) will be key elements in the analysis.

This results section is subdivided into three main parts. The first part will focus on the evolution of several morphodynamic features within the estuary, whereas the second part will focus on the evolution of the hydrodynamic features. The third part is a combination of the first two parts and will go more into detail on the combined evolution of the hydro- and morphodynamics.

4.1 Morphodynamic results

4.1.1 Large-scale morphology

The large-scale morphological evolution of the estuary under the influence of a tidal barrage is characterized by intense channel deepening in the near-field (in and around the mouth and tidal barrage) (figure 15). In the runs without unlimited maximum mouth depth, the depth increases by up to 8 meters, dependent on the degree of local width reduction and tidal barrage location (section 4.1.4). The initial channel pattern at t=0 changed around the tidal barrage and visible relocation of channels and bars is visible up to around 2 km from the tidal barrage in figure 15. Most of the changes in the relocation of the channels already takes place in the first two timesteps of morphodynamic modelling, which is 0-8 years (Appendix C). Although most of the activity in the morphologic evolution takes place directly after implementation of the barrage, the inlet still deepens in the last half of modelling time (middle and right panel, figure 15).

Next to the part near the barrage, channels in all parts of the basin become deeper (far-field). This holds true for the channels in the constant width part in the lower estuary near the sea-estuary boundary, but also for channels in the middle estuary. Patterns are equal for other runs, with larger effects when larger (changes in) tidal prisms are involved.

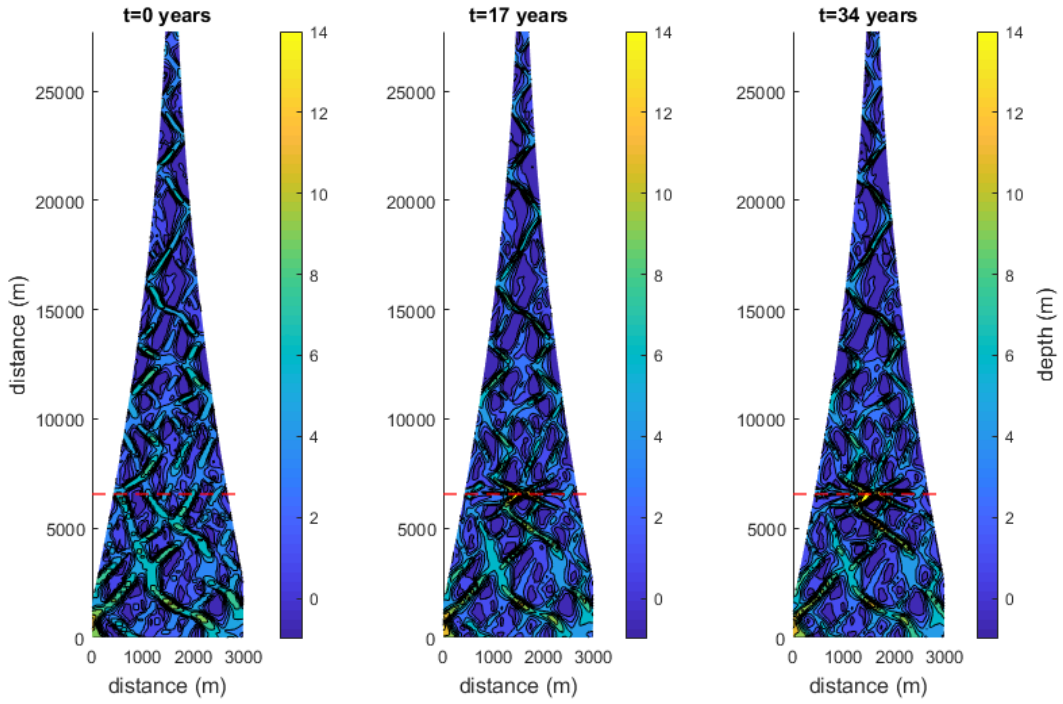

Figure 15, Evolution over time of intermediate run Cls_75_25. Red, dashed line represents location of tidal barrage at relative position 0.25, with width reduction of 75%. Presented bathymetries have been widened for the sake of visibility/readability. Figure with correct width to length ratio will be provided in thesis. More timesteps of basin evolution included in Appendix C.

4.1.2 Near-field morphology and near-field morphodynamics

The near-field morphology is characterized by deep barrage mouths with several deep channels connected to the deepest parts. The deepest parts of the mouths in all tested runs are localized directly adjacent to the thin dams, and not in the center of the mouths (figure 16). This can be explained by the fact that the water that flows along the barrage towards the mouth, meets here with the water that flows perpendicular to the barrage through the center of the estuary. The flow has to adapt to this situation by either accelerating, eroding the bottom, or both. The deepest channels are found in the bottom half of the modelled estuary and this is believed to be related to how the tide propagates along the coast in the sea part of the model.

The effects of mouth deepening are not visible in model run limited maximum depth around the barrage (Cls-75-25-LD(1)) (bottom right panel in figure 16). In this case the deepest locations are found just seaward and landward of the non-erodible layer in the subsurface. The non-erodible layer in this run is implemented at a depth of 7 meters. In contrast to the runs with unlimited maximum depths, the deepest parts (scour holes) are positioned in the center of the estuary and are much deeper (up to 25 meters). The central position of the scour holes could be explained by the reduced friction over the non-erodible model bottom around the barrage. On the model boundaries, of which the non-erodible subsurface layer is one, the shear stress is neglected, and the slip condition is “free”. This implies that the flow over the non-erodible layer or closed model boundary does not experience shear stress. This explains the flow through the estuary center and the position of scour holes along the estuary centerline. It also partly explains the depth of the scour holes, as on of the sides of the scour holes is frictionless.

The braiding index, which is the number of separate channels per estuary transect separated by intertidal area, decreases in all the mouths to 1. Just landward and seaward of the mouths the braiding index quickly increases again to its original value, measured at the same moment in (modelling) time without the presence of thin dams in the model (Cls-0-0).

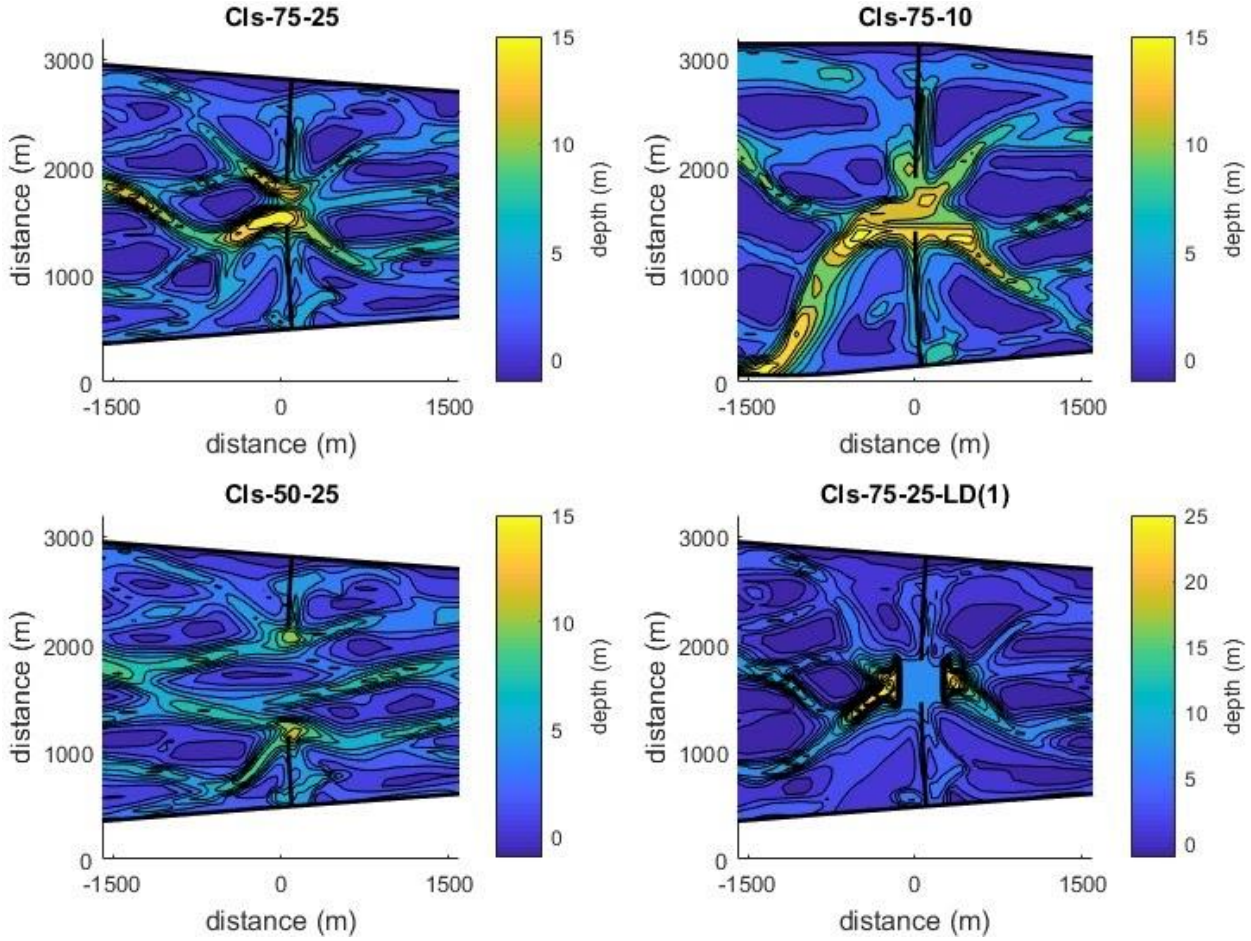

Figure 16, final bathymetry after 34 morphodynamic years of 4 model runs. Reference run Cls-75-25 is compared to runs with varying thin dam position (Cls-75-10), thin dam width reduction (Cls-50-25) and presence of non-erodible layer in the subsurface in and around the tidal barrage to limit maximum depth (Cls-75-25-LD(1)). Channels and shoals are in correct length to width ratio (1:1). Note different colorbar scale for subplot on bottom right, as deep scour holes with a depth of up to 25 meters occur just landward and seaward of the non-erodible layer.

The most important changes in near-field morphology with respect to the control run without a tidal barrage present are depicted in figure 17. Next to the changes in overall erosion and sedimentation patterns (top row), these changes concern the mean transect depth (middle row), mean channel depth (middle row) and braiding index (bottom row). The areas of intense erosion (figure 17, top row) show similarities to the final bathymetry of the model runs in figure 16. The areas dominated by deposition (blue in figure 17), are harder to recognize in the final bathymetry of figure 16. There are areas of up to 10 meters deposition. These areas are positioned in the vicinity of the new and deepened channels. The more seaward the location of the tidal barrage, or the stronger its width reduction, the stronger and larger become the erosion and sedimentation patterns. From the erosion and sedimentation patterns it also becomes clear that the new channels diverge away from the mouth at an angle of approximately 45 degrees. Most of the deposition takes place in between these deepest channels and the barrages.

Sometimes even sedimentation in the barrage mouth can take place (Cls-50-25). The mouth in this run is characterized by two separate deeper parts, located adjacent to the barrage parts. In between these two deeper zones, a relatively shallow (minimum depth = 0.5 meter) zone exists where net sedimentation has occurred over the entire modelling period of 34 (morphodynamic) years.

Special behavior can again be observed in the model run with limited maximum depth (Cls-75-25-LD(1)) (figure 17, right column). In this run the erosion in the scour holes is up to twice as large as in the other runs, in contrast to the deposition, which does not strongly deviate in maximum values from the other runs presented. The intensely eroded scour holes are also visible in the change in mean depth and mean channel depth per transect. The intense deepening effect that they have also triggers extra deposition just around the tidal barrage outside of the channels compared to the other runs (figure 17, middle row).

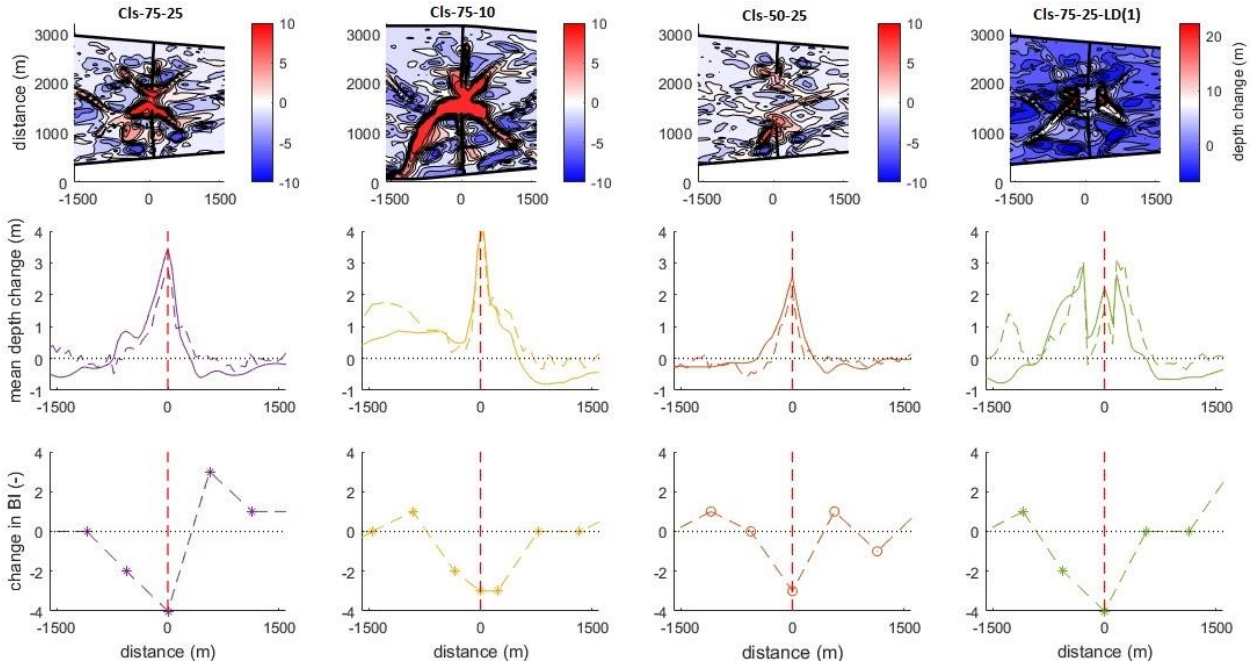

Figure 17, differential morphological plots for barrage areas. Top row represents changes in bathymetry after 34 (morphodynamic) years of modelling time, with erosion in red and deposition in blue (with respect to Cls-0-0). Second row represents the change in mean depth (solid line) and change in mean channel depth (dashed line) over the period 34 years morphodynamic years (with respect to Cls-0-0). Maxima indicate peaks in (channel) deepening and erosion, while minima indicate peaks in shallowing (of channels). Bottom row represents the change in braiding index (BI) with respect to the control run (Cls-0-0). Braiding index is the number of channels per transect separated from each other by the presence of intertidal area.

All the model runs are characterized by the same pattern with respect to mean depth change (figure 17, middle row). This pattern involves an increase of the mean depth in the barrage mouth, with areas of decreasing mean depths and channel depths in the vicinity of the barrage. In general, this tendency is stronger for mean depths (solid line) than for mean channel depths (dashed line). Mean channel depts also have the tendency to become deeper landward of the 75% width reduction barrages (purple, yellow, green). In the case of the yellow run (Cls-75-10) increased channels depth can be observed from the modelled tidal barrage up to sea part of the model.

The braiding index (figure 17, bottom row) decreases to one (single channel) in all runs, except for Cls-50-25. Here the braiding index remains at two because of the bar present in the barrage mouth. The effect in the braiding index disappears quickly with distance away from the inlet. In some of the runs the braiding index locally even increases with respect to the control run (Cls-0-0) in response to barrage placement.

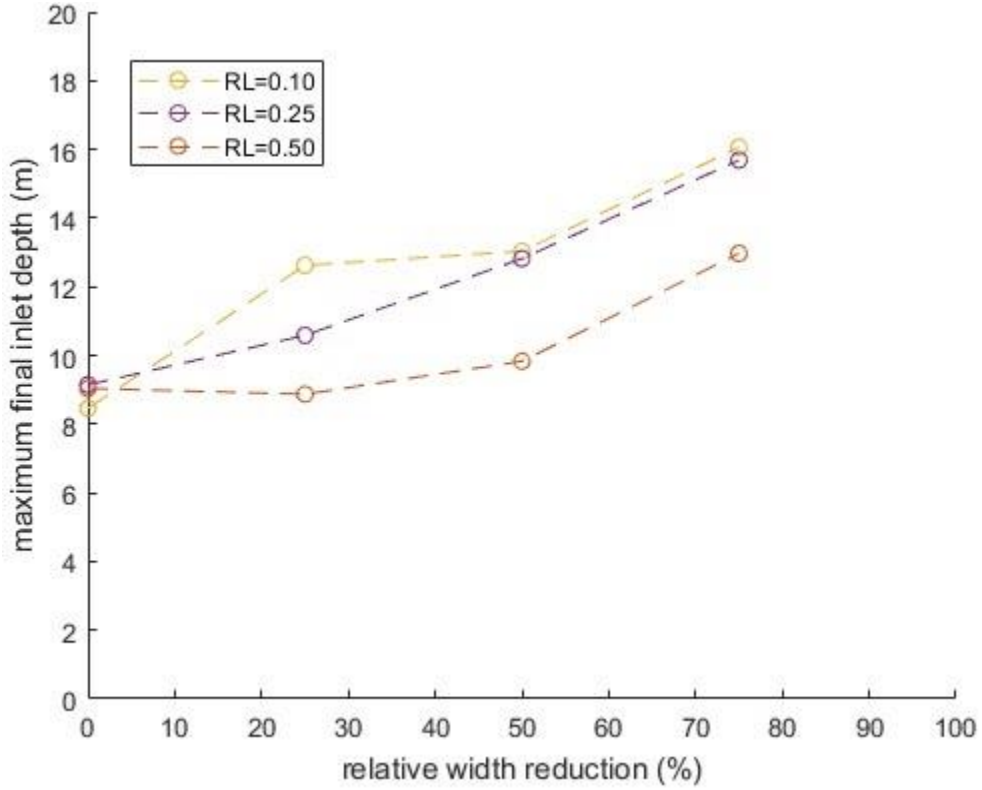

Figure 18, relative local width reduction to maximum final mouth depth plot. Points plotted for width reduction=0% represent the maximum width without barrage implementation/local width reduction at the same locations (Cls-0-0). Points are grouped in three groups based on relative location (RL) of the modelled barrage. RL is based on the total length (approximately 28 km) of the estuary from sea/estuary boundary to estuary/river boundary. Limited maximum depth runs are excluded.

Both relative width reduction as well as relative barrage location show a direct link to maximum depth of the mouth (figure 18). The data points that deviate from this pattern was generated in the absence a tidal barrage (relative width reduction=0). With increasing width reduction, the morphodynamic response has an increasing tendency of deepening the barrage mouth. The deepening of the barrage mouth and channels in the vicinity is the most pronounced response in the morphology and grows over time. As this response grows over time (at decreasing rate), the response in tidal prisms (section 4.2.1) and water level (section 4.2.2) decreases. The maximum mouth depth is linked to the total mouth cross-sectional area, of which the evolution over time is depicted in Appendix E.

4.1.3 Summed channel width

The summed channel width (figure 18) shows the same pattern as the mean depth and mean channel depth in figure 17. In the barrage mouth the maximum summed channel width is limited by the presence of the barrage. Directly adjacent to the barrage the channels (everything below the low water line) takes up all the space available per transect. Just seaward and landward of this area of increased summed channel width, the summed channel width decreases relatively to the situation without barrages (blue line). From figure 19 it is expected that area within the intertidal zone (section 4.3.2) and Vs/Vc ratio (section 4.3.3) increased around the modelled tidal barrages.

Just like in figure 18, patterns are strongest for model runs with the largest degree of width reduction and grow stronger towards the sea. This is coupled to the local responses in tidal prisms involved. As the absolute (response in) tidal prism increases towards the sea and with increasing relative width reduction, the (response in) observed morphology also grows larger.

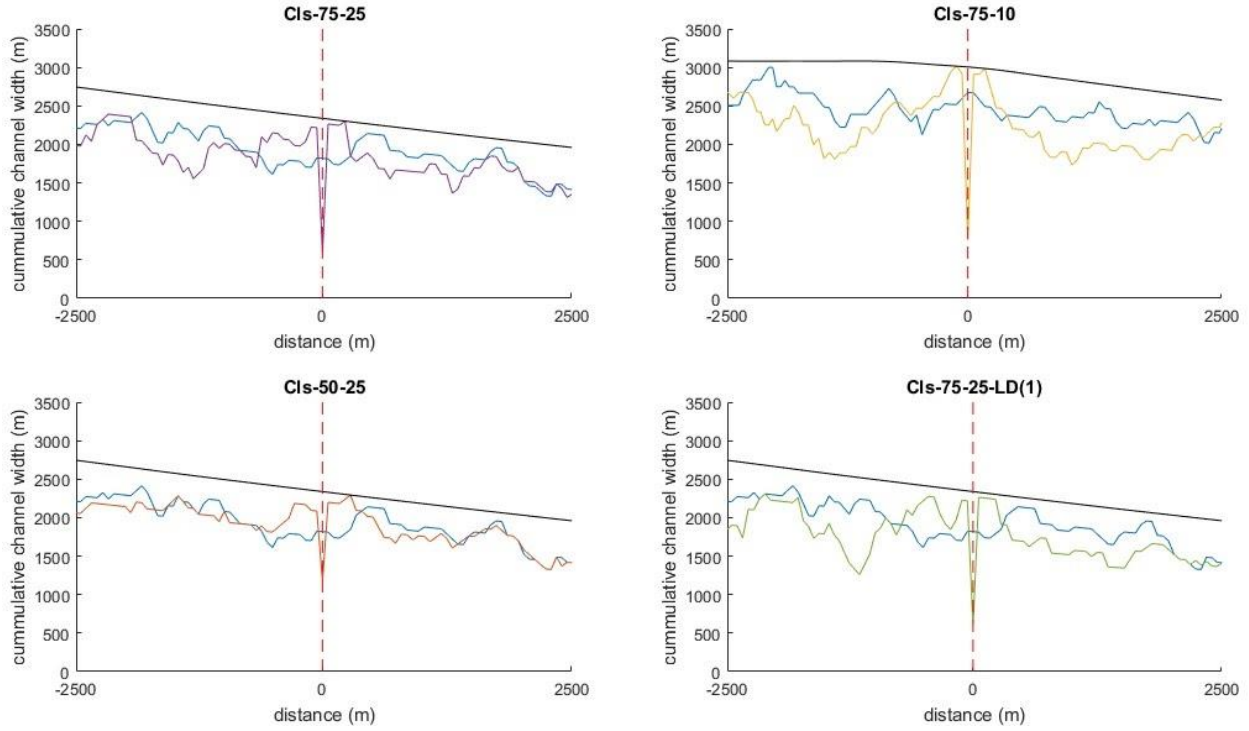

Figure 19, cumulative channel width and local maximum estuary planform width at the end of modelling period (t=34 years). Red, dashed line indicates the location the thin dam. Black solid line indicates the maximum local estuary planform width. Blue line indicates the final situation without thin dam (Cls-0-0 at t=34 years). Solid, purple/yellow/red/green lines indicate the local cumulative channel width after 34 morphodynamic years. Area that is not classified as channel is classified as intertidal area. Boundary between channel and intertidal area is set at the offshore low water line (-1 meter) and is kept constant over time and distance for the sake of continuity.

4.2 Hydrodynamic results

4.2.1 Tidal prism

The response in tidal prism to the placement of the tidal barrages decreases over time (figure 20, bottom row). The hydrodynamic response to the placement of the barrage is direct (strongest after first timestep) and its magnitude decreases over time for all model runs, except the ones with maximum limited depth around the barrage. The strongest reaction in tidal prism, as well as in morphodynamics, to barrage placement is shown by Cls-75-10. The smallest response is shown by Cls-50-25, also in correspondence to hydrodynamic results.

The overall effect in absolute tidal prism value remains in the order of a few percent (max 3%) (top right panel figure 20). And the relative tidal prism difference remains relatively constant over distance. No clear response in the pattern of the tidal prism decrease to tidal barrage location can be deduced form the data in figure 20. But it is clear that the Cls-75-10 tidal prism reduction is stronger for all data points than the Cls-75-25. And so, propagation of the tidal wave into the basin must be hindered more in the situation with the most seaward positioned tidal barrage.

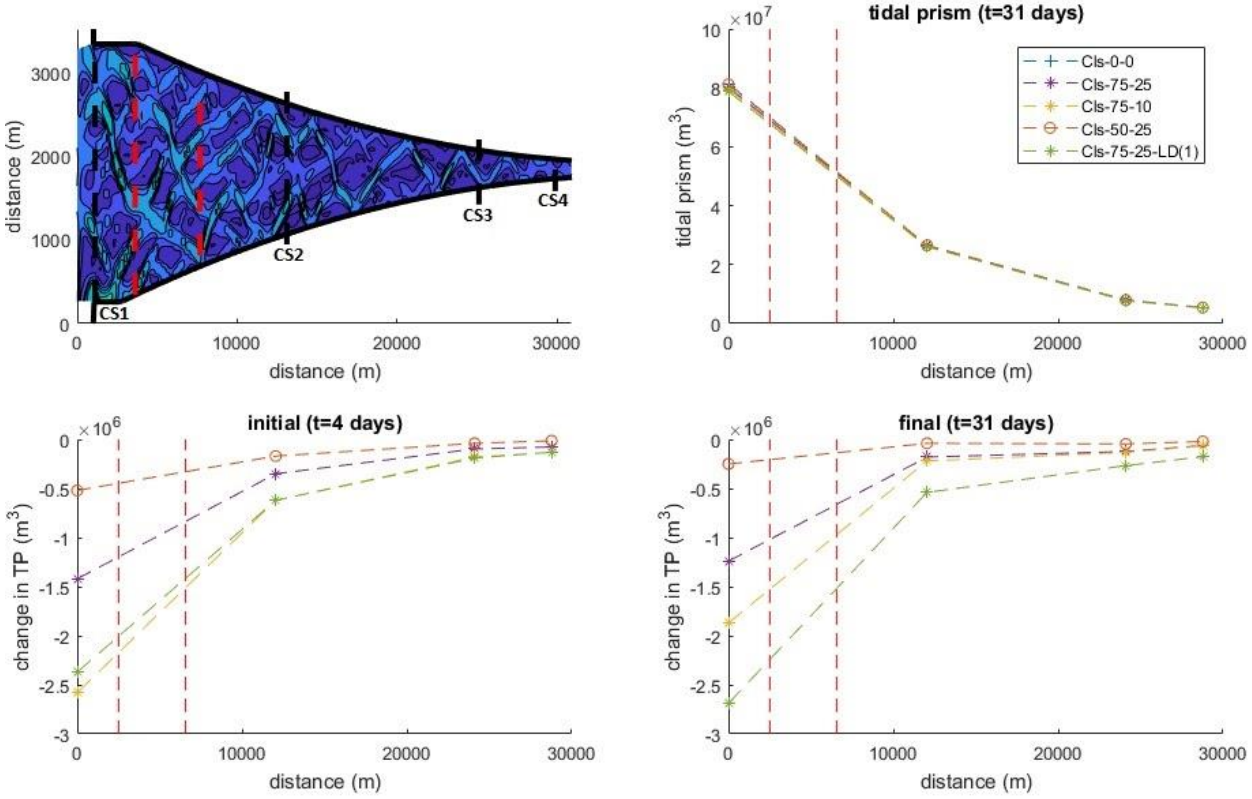

Figure 20, tidal prism and changes in tidal prism under the influence of local width reduction and barrage location. Top left panel indicates positions of cross-sections (CS) and hydrodynamic measurement points (at some location) included in other panels with black, dashed lines. Red, dashed lines indicate positions of thin dams involved at RL=0.10 and RL=0.25. Morphology in the top left panel is compressed in horizontal direction and represents initial bathymetry used in all model runs. Top right panel indicates the tidal prism after the entire modelling period (t=31 hydrodynamic days). Bottom row figures indicate the change in tidal prism with respect to the situation without thin dams, after 4 hydrodynamic days (timestep 1/initial response) and after 31 hydrodynamic days (final timestep).

The tidal prism response to the tidal barrage with limited maximum depth even slightly increases over time. This is despite that the barrage CSA also increased over time in this model run. The tidal prism response of the Cls-75-25-LD(1) might be triggered by another morphodynamic response than just deepening of the inlet. The erosion of material from the scour holes and from entire limited depth area is coupled to increased deposition seaward (and landward) of this area. Coupled to the decrease in summed channel width (figure 19), decrease in mean depth (while the mean channel depth increased) (figure 18), this could imply an increase in tidal flats in the area seaward of the barrage. The increased intertidal area and narrower channels could impede the propagation of the tidal wave into the estuary. More attention will be paid to the role of the intertidal area in sections 4.3.1 and 4.3.2.

4.2.2 Water level

Just like for the tidal prisms, the water levels are also affected by the presence of the placement of the tidal barrages. Once again, the hydrodynamic response is stronger right after the placement of the tidal barrage and decreases over time as the morphodynamic response becomes more pronounced (figure 21). Both the high and low water show the same pattern in response of the different model runs. With the strongest responses in runs Cls-75-25-LD(1) and Cls-75-10. As expected from literature (Wolf et al., 2009), the tidal range decreased in all tested situation. The maximum decrease in tidal range is about 7 cm, which is also in the order of a few percent of the total offshore tidal range. The response of the Cls-75-25-LD(1) remains large over time as the near-field morphology is not able to respond to the barrage placement by channel deepening and mouth CSA increase (figure 17).

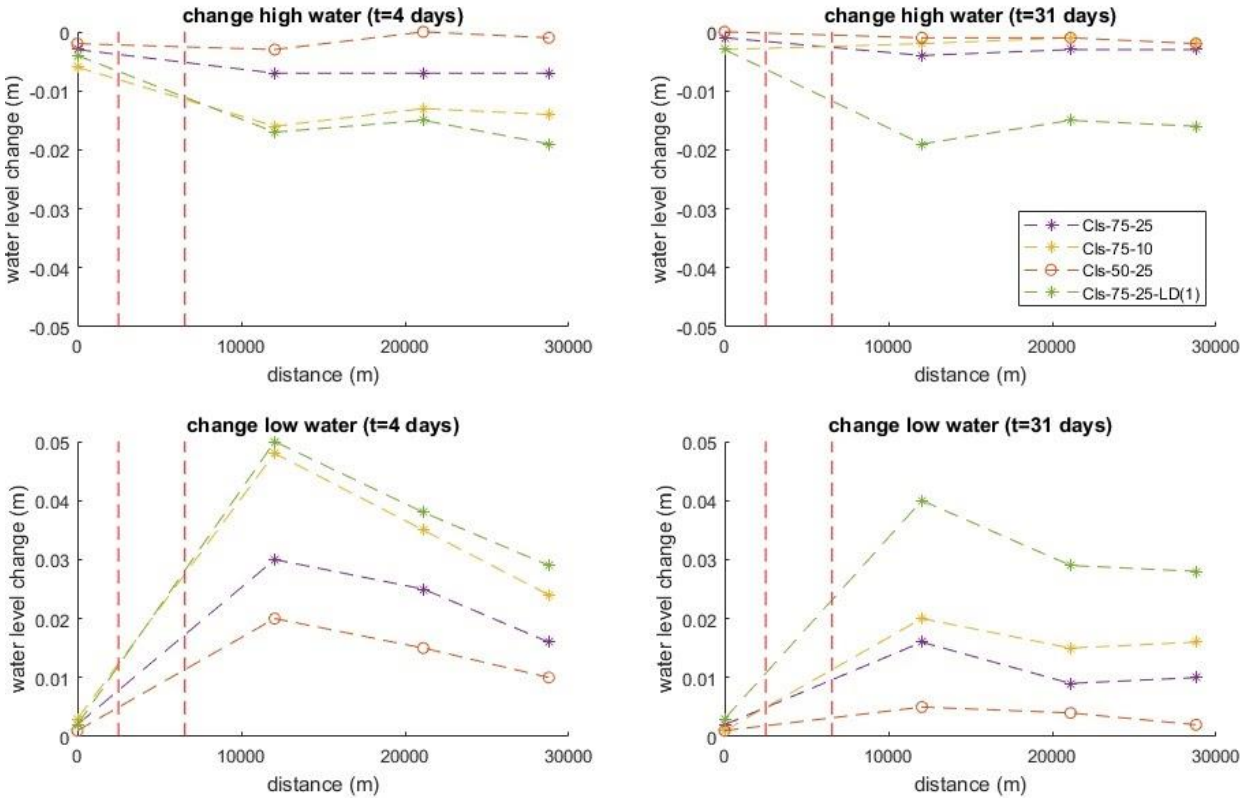

Figure 21, changes in high water level (top row) and low water level (bottom row) with respect to situation without tidal barrage (Cls-0-0). Left column represents the initial hydrodynamic (at timestep 1) response of the system to barrage implementation, whereas right column represents the change after the entire modelling period of 31 hydrodynamic days. Red, dashed lines indicate the positions of the thin dams involved, at RL=0.10 and RL=0.25.

The compression of the tidal range is an important consequence of the barrage placement as many regions that were initially intertidal would classify afterwards as subtidal (or supratidal in natural systems with higher elevated tidal flats). This would have consequences for intertidal ecology in the affected regions. For some of the UK estuaries around the Irish Sea, this would be an important result as the ecology here is one of the most important aspects hindering the implementation of large-scale tidal energy schemes (Cooper et al., 2009).

4.3 Combined hydro- and moprhodynamic results

4.3.1 Cumulative sediment transport

The link between the morphodynamic and the hydrodynamics features analyzed in this results section are the sediment fluxes. The net residual sediment transport patterns can be driven by different factors. To keep things simple the cumulative transport fluxes will first be analyzed and later combined with the estuary morphology to draw conclusions on the nature of the sediment transport.

The initial positive cumulative transport peaks in cross-sections 1 and 2 are not directly related to transport asymmetry of any type. Instead the spin-up period of the model seems to trigger the sudden large landward sediment flux. More important for the analysis of the transport asymmetry are the trends all the cumulative transport fluxes show (figure 22). From the trends all the tested barrage situations show, it could be concluded that the whole basin is ebb-dominated. For cross-section 4 the material is originating from the tidal river bed and the transport is dominated by seaward directed residual/river flow. The same largely holds true for cross-section 3.

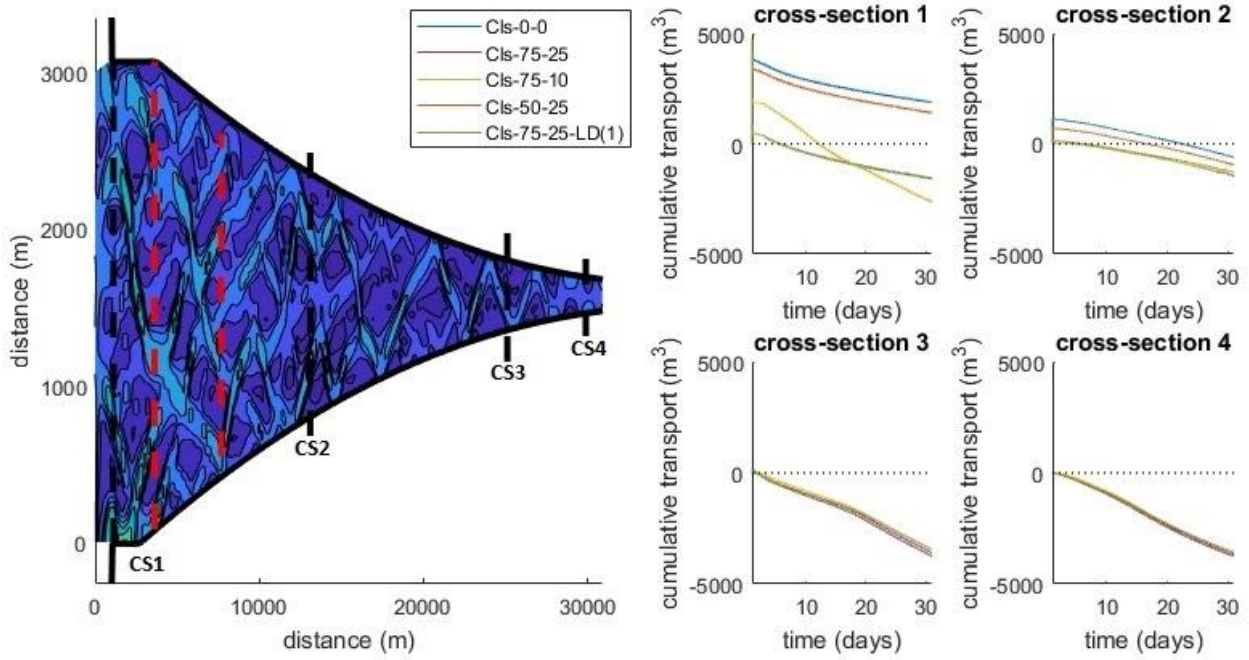

Figure 22, cumulative sediment transport through 4 cross-sections. Cross-sections (black, dashed lines) and relevant thin dam positions (red, dashed lines) are indicated in the left panel. Bathymetry in left panel is initial/equilibrium bathymetry of all model runs and is strongly compressed in horizontal direction. Positive(/negative) values in the right panels indicate cumulative landward(/seaward) directed transport. Entire modelling period of 31 hydrodynamic days is presented in right panels.

Striking is that the situation without tidal barrage present (Cls-0-0) is most flood-oriented in both cross-section location 1 and 2 (figure 22). So, the increased channel depth (figure 17), and locally decreased summed width of channels (figure 19) stimulates the ebb-dominant transport. This is in line with what the ebb-dominated morphology is expected to look like (Friedrichs and Aubrey, 1988). Important to note is that the ebb-dominated transport decreases over time in magnitude in cross-section 1, while it increases in cross-section 2. The modelled tidal barrages are located in between these two cross-sections. In the next section the morphodynamic changes of in the lower estuary will be discussed in more detail based on the a/h and Vs/Vc ratios, in order to gain some more insights in how the tidal barrage influences the transport fluxes.

4.3.2 Area within the intertidal zone

The modelled barrage placement overall has a slightly positive effect on the area present within the offshore defined intertidal zone (figure 23). It must be emphasized that the intertidal area in this section comprises everything with an elevation above the low water line. This boundary was chosen, because no elevation exceeded the high water line at any moment and to be able to easily draw comparisons between the intertidal area at different moments in time. Sedimentation on the intertidal flats generally occurs by the action of tides. And so, sedimentation on the tidal flats and increase of the total intertidal area were expected to happen as there are no waves present in the model to erode the tidal flats.

In the case of Cls-75-25 (purple) it becomes clear that intertidal area predominantly grows just seaward of the barrage and in the upper estuary (figure 23, top right panel). Whereas it disappears in the formation of the new channel network around the barrage mouth. Striking in the evolution of the intertidal area for the entire estuary (EE) is the Cls-0-0 run (blue bars). The evolution of the estuary without tidal barrage present still results in a slight increase in total intertidal area (Cls-0-0i and Cls-0-0f). Next to that, the 50 percent width reduction run (Cls-50-25) does not result in a different observable response according to figure 23 from the situation without a barrage in place (Cls-0-0f). The runs with 75% width reduction do show a clearly observable pattern of increase in intertidal area (Cls-75-25, Cls-75-10, and Cls-75-25-LD(1)), although the barrage position is important.

In the vicinity of the barrage the intertidal area increases, while in subsection not adjacent to the barrage the evolution of the intertidal area follows the same trend as the situation without barrage (Cls-0-0f). This is observable in the top right panel of figure 23. Here the area around the barrage is characterized by relation of channels and bars, whereas further away the deposition takes place on the edges of the intertidal areas that were already present. Striking are especially the peaks in subsections 1 and 2 for run Cls-0-0 (yellow). This in combination with the channel deepening observed in figure 17, will locally result in more ebb-dominated morphology with deeper and narrower channels. The deepening of the barrage mouth and the channels between the sea and the barrage mouth could potentially influence the tidal propagation into the estuary. The discussion section will go deeper into the possible implications.

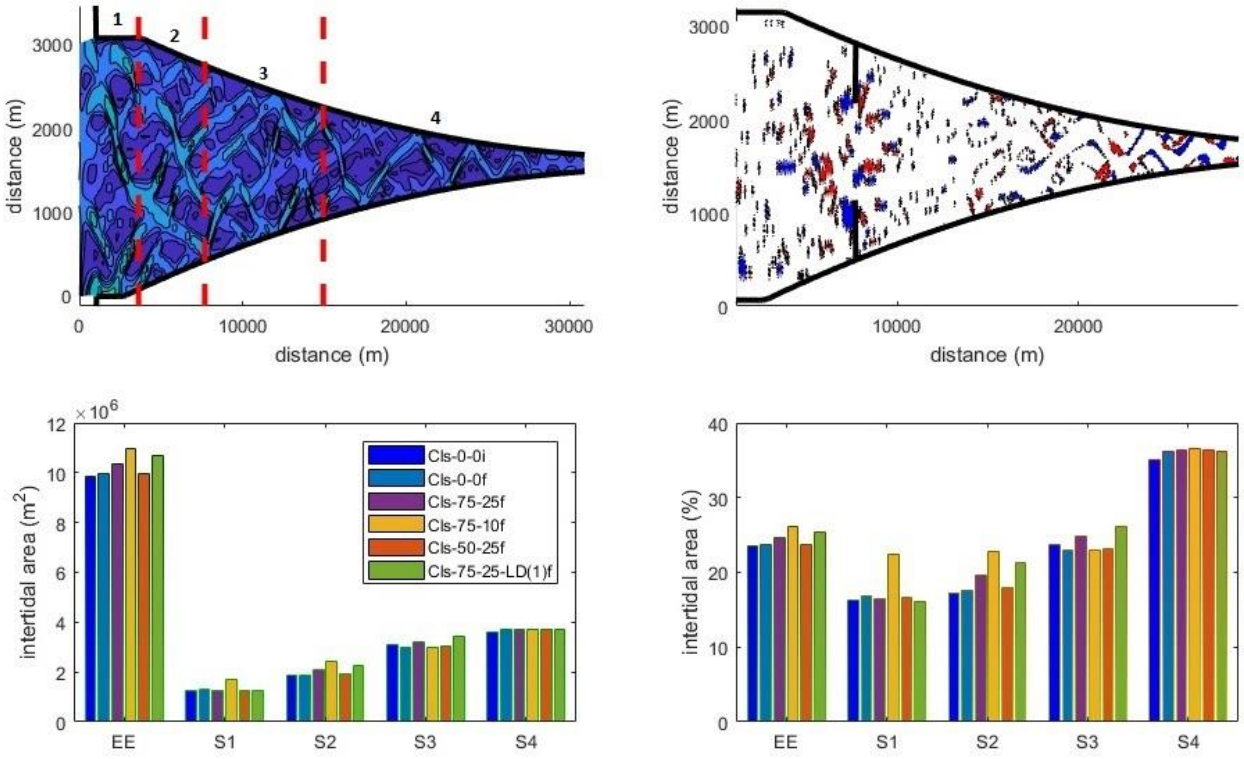

Figure 23, intertidal area for the entire estuary (EE) and for the previously presented four subsections (S1-S4). Letters "i" and "f" in legend represent initial and final situations. Top right panel indicates the locations in the reference run Cls-75-25 where intertidal area has grown (blue) or disappeared (red) over the entire modelling period of 34 morphodynamic years.

The limitation of the maximum depth around the modelled barrage has a positive effect on the intertidal area around the barrage (Cls-75-25 and Cls-75-25-LD(1) in figure 23). This could partly be explained by the deposition of the extra material eroded from the scour holes and the formation of a deeper central channel seaward of the modelled barrage accompanied by a local decrease in summed channel width (figure 17).

The slight increase of the intertidal area in subsection 4 is a result the surplus of sediment transported through cross-sections 3 and 4 in combination with the only mildly ebb-dominated transport through cross-section 2. The position of cross-section 2 almost coincides with the positions of the barrage location 0.50 (figures 14, 22, and 23). The material coming from the tidal river through cross-sections 3 and 4 (figure 22) is not completely transported into subsection 3. This in combination with the increased downstream sediment transport by barrage placement through cross-sections 1 and 2 causes sediment starvation in subsection 3, according to the decrease in intertidal area. This sediment starvation is irrespective of barrage placement. The increase in intertidal area for runs Cls-75-25 and Cls-75-25-LD(1) is merely a result of nearby barrage placement and channel deepening/narrowing.

4.3.3 Basin geometry, a/h ratio, and Vs/Vc ratio

In general, the responses in basin geometry are strongest in the direct vicinity of the modelled tidal barrages. The responses include an increase in Vs/Vc ratio near the modelled tidal barrage in the order of a few percent and a decrease in a/h in the order of a few percent (figure 24). In the subsections that do not directly border the modelled tidal barrage the Vs/Vc ratio remains relatively constant and a tiny increase in the a/h ratio can be observed. Depending on the vicinity of the modelled barrage, the a/h ratios change with respect to the situation without modelled tidal barrage (blue cross). Far away from the modelled barrages, the a/h ratios slightly decrease, while in subsections directly next to the modelled barrages the a/h ratios decrease.

The Vs/Vc ratio essentially represents the ratio between volume of intertidal storage (Vs) to water stored in the channels (Vc) at mean sea level. The volume of intertidal storage can increase by either increasing the intertidal area or the water stored in the intertidal area. The Vs/Vc can also increase by a decrease of the water storage in the channels. However, this is unlikely as in general channel deepening was observed (figures 15 and 17) and the a/h ratio increase is limited for all subsections presented in figure 24.

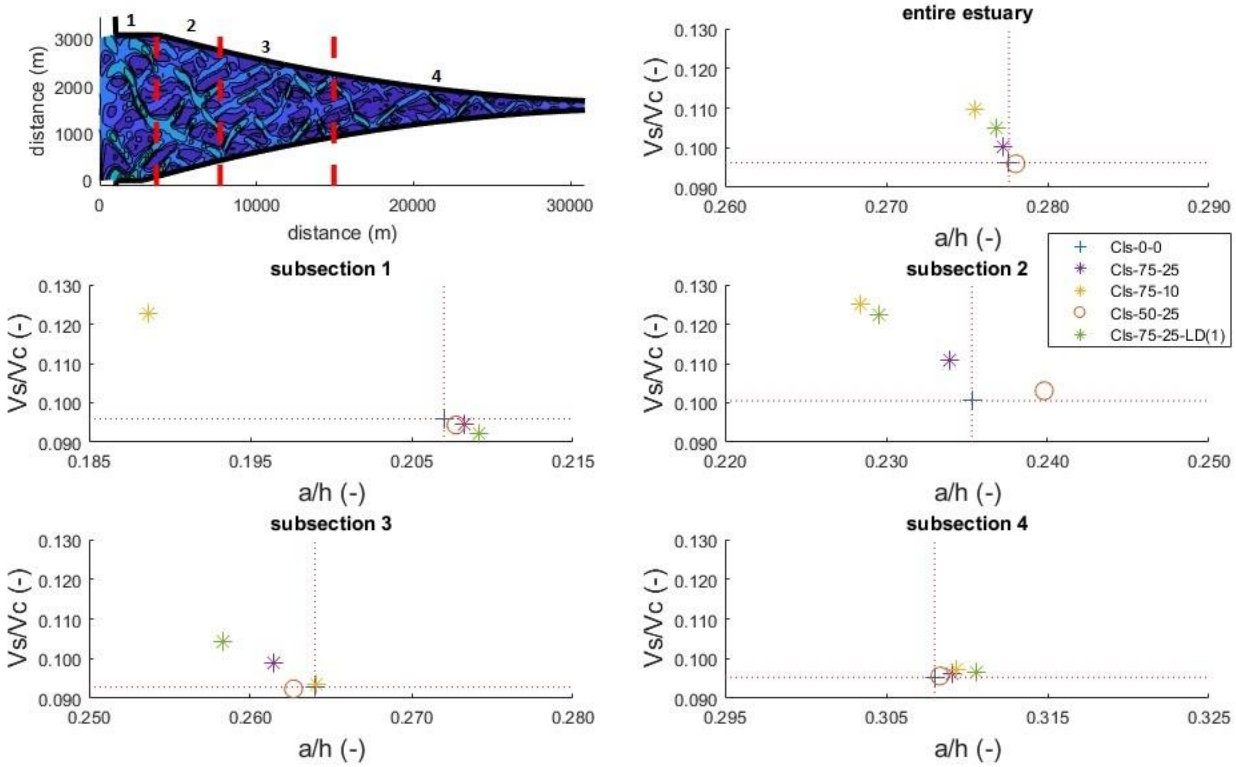

Figure 24, a/h to Vs/Vc figure indicating the ratios between the offshore tidal amplitude (a) to mean local channel depth (h), and volume of water stored in the intertidal area (Vs) to the volume of water stored in the channels (Vc). Ratios are provided for the entire estuary, as well as for the estuary subsections, which are indicated by the numbers in the top left panel. Red dotted line indicates the local value of the ratios per section for the situation without thin dams (Cls-0-0). Red, dashed lines that separate the subsections from each other indicate tested thin dam positions. Bathymetry shown in top left panel is the initial/equilibrium bathymetry and is strongly compressed in horizontal direction.

From figure 22 it became clear that based on cumulative transport patterns, the modelled estuaries are ebb-dominated. Ebb dominated estuarine morphology is usually characterized by narrow deep channels and extensive tidal flats. Normally this would be represented by a relatively large Vs/Vc ratio compared to the a/h ratio. This does not entirely hold according to where the datapoints from figure 23 would plot

in figure 7. It is certain that in general the modelled estuaries under the influence of the tidal barrage move to stronger ebb-dominated morphology. The initial bathymetry is already characterized by relatively deep channels and the further deepening is enforced by the placement of the modelled barrage (figure 14, figure 15, and figure 17). Because of the ebb-dominated character of the modelled estuaries (figure 22), the system loses sand to the sea that is only supplemented by sand from the tidal river bed (figure 22, cross-section 4). Sediment starvation seems to affect the entire basin, but effects are most visible in the middle estuary (subsection 3). The effects are expected to spread over time and become visible in the morphological features. It is not unexpected that sediment starvation occurs, as no sediment is imported into the system by the river. But an important result is that the placement of the tidal barrage seems to reinforce the effects of the already ebb-dominated morphology in the movement of sediment towards the lower estuary and sea.

The same pattern in response to the modelled barrage placement can be observed in figure 24 as in other hydrodynamic and morphodynamic features. The strongest morphodynamic response is generated in the Cls-75-10 run (yellow star). Especially in subsection 1, which is positioned in between the barrage and the sea-estuary boundary in this model. In subsection 1, deep channels form between the barrage mouth and the sea, strongly decreasing the a/h ratio. In combination with the decrease in a/h, an increase in Vs/Vc can be observed which is surprising considering the large seaward directed cumulative sediment transport through cross-section 1 (figure 22). It is believed that the tidal flats in subsection 1 are supplemented by material moving seaward from subsection 2 and 3 (figure 22).

5. Discussion

Firstly, in this discussion chapter, an interpretation of the results follws and the interpretation will be coupled to literature presented in the literature review chapter. Secondly, the implications of this for science and society will be discussed in combination with suggestions for further research in this direction.

5.1 Interpretation of morphodynamic results

Firstly, an interpretation of the results presented the morphodynamic results section, which cover the overall basin morphological evolution, near-field erosion and sedimentation patterns, mean depth, mean channel depth, summed channel width, and braiding index.

The most important morphodynamic response lies in the channel depth increase (figures 15, 17, and 18). This is also the most important effect that came forward in the literature review (Retiere, 1994; Cooper, 2009; Wang, 2010). Directly coupled to the increased channel depth, is the increased depth of the barrage mouth and consequently the barrage mouth CSA. Figures 15 and 17 show that the initial channel network around the newly placed barrages was abandoned and by intense erosion two new channels formed. These new channels were linked to the mouth at an angle of around 45 degrees from the estuary centerline (figure 16). The channels were not just linked to the new depression that was formed in and around the barrage mouth, but rather to the deepest parts of the mouth that were positioned on both sides of the mouth right next to the modelled barrage parts. This led to the observation that if the mouth is too wide, sedimentation could occur within the barrage mouth, as was the case in model run (Cls-50-25). This sedimentation could potentially hamper the tidal barrage functionality.

Besides an increased mouth depth, the summed width of channels also increases around the barrage and locally takes up the whole estuary planform width (figure 19). So, the depth increase is not only restricted to the mouth itself but also the surrounding area. Removal of intertidal area from the mouth and surrounding areas, in combination with deepening of the mouth area, could in natural estuaries cause problems with flooding higher up in the estuary (Leuven et al., 2019).

Up to several kilometers distance from the barrage, the channel pattern was altered considerably by the the placement of the modelled tidal barrage. A possible consequence would be the relocation of tidal flats in the vicinity of the barrage (Retiere, 1994). This would probably affect the local ecology, but this will restore as the overall area in the intertidal zone slightly increased by the placement of the modelled tidal barrages. It could however cause problems if certain patches of tidal flats comprise protected ecology like the Bollen van Ooster near Lake Grevelingen. It is expected that these tidal flats, which are part of the Natura2000 initiative, will partly erode as a result of the reopening of Lake Grevelingen (Wang, 2010).

5.2 Interpretation of hydrodynamic results

The most important hydrodynamic results involve a decrease in tidal range and consequently the compression of the intertidal zone. The decrease of the tidal range is a result of the decrease in tidal prism. The normal propagation of the tidal wave into the estuary is impeded by the tidal barrage. Although the water levels are influenced (up to 7 cm reduction), the response in the tidal prism to the tested barrages is relatively mild (up to 3 percent). These changes are small compared to the decreased high-water levels

found by Xia et al. (2010) of up to 1.5 m in the landward part of the Severn estuary (up to 13% of tidal range). The reduction in high water levels was accompanied by a maximum decrease in tidal prism of 30-50% (Xia et al., 2010). The response in tidal range is largest right after placement of the modelled barrage (timestep 1). Over time the hydrodynamic response decreases as the morphology adapts to the new situation. The hydrodynamic response remains constant when the barrage bed would be fixed by making use of non-erodible layer in and around the barrage mouth. This would be expected to be incorporated in a newly constructed tidal power plant in a natural system. The compression of the intertidal zone is mentioned by Wolf et al. (2009) as an important effect of tidal energy scheme emplacement and harmful to ecology.

Next to the compression of the intertidal zone, also increased slack water periods and increased mean sea level were categorized as potential hydrodynamic effects of a tidal barrage. The longer slack water period increases the tendency to seal off areas of high turbidity (de Laleu, 2009). On the other hand, longer slack water periods would decrease the turbidity and increase the light penetration which would be beneficial to the primary production by phytoplankton (Cooper et al., 2009). Increased mean sea level would affect the intertidal ecology, as it shifts the intertidal zone (Gordon, 1994; Wolf et al., 2009; Xia et al., 2010). The longer slack water periods and increased mean sea levels associated with tidal barrage placement were left out of consideration in this thesis as this would complicate the numerical modelling.

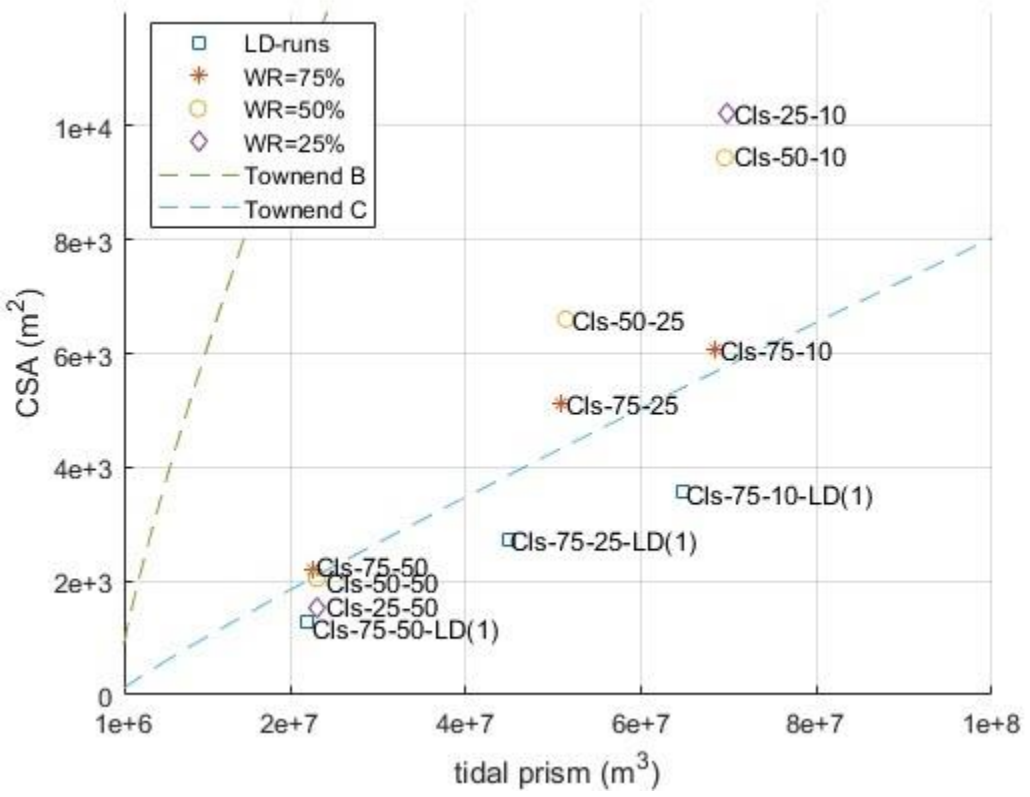

Figure 25, adaptation of Townend (2005) figure of cross-sectional area-tidal prism relation. Added to this figure are points based on final hydrology (tidal prism) and morphology (inlet area). Points are grouped based on width reduction (WR) or presence of a non-erodible layer in the inlet subsurface, and therefore having a limited (maximum) barrage mouth depth (LD). Dashed lines correspond to dashed lines as provided by Townend in his figure (Townend, 2005).

In figure 25 the morphodynamic and hydrodynamic responses are combined. Next to that, the modelled estuaries with barrages included are compared to natural estuaries, represented by the dashed lines (Townend, 2005). The most important observation from figure 25 is that the tidal prisms for the LD-runs (runs with restricted maximum depth in and around the barrage, blue squares in figure 25) remain altered with respect to the other Cls-runs. The LD-runs represent a situation in which the estuary cannot respond by increasing the CSA and therefore keeps a decreased tidal prism. This is also expected to happen in natural systems in which an actual tidal barrage is constructed. The runs with a width reduction of 25% in the barrage mouth (Cls-25-..) (purple data points), represent runs with a too large CSA, that does not trigger any response in hydro- or morphodynamics. Therefore they plot far away from the dashed line and the Cls-75-.. points (red stars). The Cls-75-.. points represent a situation in which the inlet CSA has adapted itself by depth increase to a new equilibrium state in the presence of the tidal barrage.

5.3 Interpretation of combined hydro- and morphodyanmics

With the placement of the modelled tidal barrages the channels in the vicinity of the modelled barrages deepened (figure 17). The eroded material from the channels was transported in the seaward direction (figure 22). Most of this sediment was again deposited by the action of tides on the tidal flats, which made the summed channel width (figure 18) decrease and the area present within the intertidal zone increase (figure 23). The combination of deeper channels and extensive tidal flats made the Vs/Vc ratio increase and the a/h ratio decrease in the vicinity of the modelled tidal barrages. This led to local morphology becoming more suitable for ebb-dominated transport. This ebb-dominated transport was based on the idea that in such a system, a relatively faster exchange of water through the deep channels around low tide can occur than the slower exchange of water around high tide over shallow extensive tidal flats (Friedrichs and Aubrey, 1988).

The already deep, ebb-dominated system became even deeper by the implementation of the modelled tidal barrages, and this reinforced the already existing ebb-dominance. The result that the system exhibiting a profound tidal asymmetry can only remain flood- or ebb-dominant, is in accordance with the findings of Friedrichs and Aubrey (1988).

In the upper estuary the effects of the tidal barrage placement are limited. The limited measured effects in the middle and upper estuary could partly be explained by the limited time for which the model has run (34 years), compared to other morphodynamic models, which run for hundreds or thousands of years in modelled time. The morphological changes further away usually take more time as the observed changes generally slowly move through the system (Van Maanen et al., 2013; Nnafie et al., 2014; Nnafie et a., 2018). If sediment would have been added to the river discharge in the model, more changes in morphology in the upper estuary would have been observable. Morphologic changes that are now triggered by the barrage and move upstream from the tidal barrages, could in that case also move downstream from the tidal river.

5.4 Consequences of findings for research questions

The findings of this thesis, on the large-scale morphodynamics of an estuary under the influence of tidal barrage placement, indicate that implementation of a tidal barrage has consequences for estuarine morphology. Many of the results confirm the outcomes of modelling studies (Wolf et al., 2009; Xia et al., 2010), empirical studies (Retiere, 1994), or literature studies (Wang, 2010) conducted into this field of research.

The most important results found, with respect to the research questions, are that the degree of width reduction and position of the width reduction within the estuary strongly influence the hydrodynamics, sediment transport, and resulting morphology. The alteration of the hydrodynamics can most easily be observed in the compression of the intertidal zone by reduction of the tidal range. This has consequences for the local tidal prism and cumulative sediment transport. The strongest changes in morphology are mainly triggered by another alteration in the hydrodynamics, which is the increase in maximum flow velocities around the width reduction. This results in very deep barrage mouths, or even scour holes, where the maximum mouth depth was restricted (LD-runs). Material that is eroded from the mouth and from the deep channels just around the barrage mouth is deposited on the shallower parts mainly seaward of the width reductions. Next to that the areas just landward and seaward of the width reductions also increase their relative storage capacity of water within the intertidal zone.

However, the implementation of a non-erodible layer does result in even stronger reorientation of the channels and bar pattern near the inlet. Moreover, as the inlet is limited in its size, the local equilibrium cannot easily be restored, and morphology over a larger distance from the barrage was influenced. This reorientation of the channel pattern is also one of the main measured/feared consequences of tidal barrage implementation (Retiere, 1994; Wang, 2010). The tidal barrage placement has a positive effect on the total intertidal area, but the compression of the intertidal zone by alterations in water levels partly outweighs this effect. Because the intertidal area analysis was based on the area between the offshore low- and high-water lines, the outcomes of the analysis overestimate the exact area that would be positioned between the new low- and high-water lines. The combined result of these two outcomes was not incorporated in the thesis, as this result would be based the extrapolation of only few hydrodynamic measurement points and would have no real meaning. In the four runs incorporated in the results section the actual intertidal would decrease by around 1% when combining the hydrodynamic effect of intertidal zone compression (decrease) and the morphodynamic effect of increase in area present within the offshore defined intertidal zone.

The total intertidal area within the basin is very important as the ecological concerns are the most important driver impeding the implementation of large-scale tidal power schemes in the estuaries around the Irish Sea (Cooper et al., 2009). Many of the intertidal areas are covered by mudflats or salt marshes which are important ecological habitats for invertebrates or winter-feeding grounds for birds. Many of these areas are therefore considered valuable (Wolf et al., 2009) and are protected under the Natura2000 initiative (Cooper et al., 2009).

5.5 How to improve this research and further research

Many features of natural estuaries have been set to a constant value or even completely left out of this project for the sake of simplicity or to be able to better study the other features. The most important of which are, river sediment, sediment type, discharge fluctuations, spring-neap cycles, and wave action. Besides, compromises had to be made on the modelling of the tidal barrages. The most meaningful improvements here could be made by holding the water for a certain time/phase of every tidal cycle to increase the relative head difference.

From a civil engineering point of view, it should be stated that for the maximum yield of an actual tidal barrage with respect to power output, optimum values could be calculated for basin and barrage parameters (Prandle, 1984). To actually fully assess the impact of tidal barrage implementation on estuarine morphology, several of this optimum values (like barrage position) in combination with several

natural processes/features (like the inclusion of mud, spring-neap cycles, and river sediment) should strongly increase the contribution of the research into the possibilities and limitations of tidal barrages.

5.6 Implications for science and society

In this report, an attempt was made to sum up the most important findings on the effect of tidal barrage placement on estuarine hydrodynamics and morphodynamics. Therefore, the hydrodynamics and morphodynamics of an idealized estuary were modelled. Bringing these things together has not been done many times before, as earlier studies focused mainly on altered hydrodynamics (Xia et al., 2010) or on observed morphology (Retiere, 1994), but not often both at the same time.

The most important implications that come forward in this thesis concern reorientation of channel pattern and shifted tidal flat positions, compression of the intertidal zone and changes in residual transport pattern all affect the intertidal flats which form the habitats of the estuarine flora and fauna (Gordon, 2008; Wolf et al., 2009). Next to that, the decrease in wave action could also change conditions for benthic organisms as it could lead to stronger stratification and could decrease the suspended matter concentrations in the water hereby increasing light penetration (Falconer et al., 2009). Retiere (1994), points out another effect for morphology, which is the complete closure of the estuary during construction. For the La Rance estuary in France, this complete closure lasted for 3 years and was devastating for the local ecology. Although many of the species could soon return after reconnection of the estuary to the open ocean (Retiere, 1994).

What has not yet been addressed so far is flood safety. The closure of an estuary by a hard structure, that could be closed off during storm events, hereby shortening the affected coastline, could potentially increase the flood safety of people living close to the estuary in the event of short periods of increased water levels (De Jonge et al., 2014). Coastal erosion and erosion of tidal flats as a result of wave action will also decrease (Friedrichs, 2011), as swell waves will no longer be able to reach the estuarine coastline. The decreased flood risk from storm events and the decrease of coastal erosion by wave action (Xia et al., 2010), could act as an additional motivator, next to the need for (new) renewable energy sources, to realize the construction of a tidal barrage in the foreseeable future.

In the Southwest of the Netherlands hard structures closing of several tidal basins are already in place and so large initial investments associated with tidal barrage placement can partly be omitted. Some of the initially marine/coastal ecology was cut off from the open sea by these impenetrable hard structures, like the Grevelingen Lake. Reopening of tidal basins like these could benefit local ecology and contribute to renewable energy generation goals, although being considered not cost-effective due to limited tidal range (Cooper et al., 2009).

6. Conclusion

In this thesis, a 2DH Delft3D model was used to study the effects of tidal barrage implementation on estuarine hydro- and morphodynamics. An idealized estuary model with only tidal forcing was used as a starting point. Locally in this model, width reductions were implemented to simulate the placement of tidal barrages. Three degrees of relative width reductions were tested (75%, 50%, and 25%) in combination with three tidal barrages at locations $^{1}/_{10}$, ¼ and ½ of the total length of the modelled estuary. For all barrage locations, combined with a relative width reduction of 75%, additional model runs were carried out including limited maximum barrage mouth depths. All models were run for the same amount of time and with all other parameter settings kept constant.

Direct after the placement of the modelled tidal barrages, a response in tidal prisms and consequently a response in tidal water levels was observable. The tidal prisms decreased up to 3%, resulting in a decrease in tidal range and a compression of the intertidal zone. The response in tidal prisms and water levels decreased again over time, but the tidal prisms and water levels did not return to their initial values over the entire modelling period.

The reason for the decrease in the hydrodynamic response was the morphodynamic response. The morphodynamic effects were predominantly observable up to a distance of a few kilometers from the barrage. The most important response was the increase in depth of the barrage mouth (8 meters) and the channels near the mouth. With the deepening of the mouth, the mouth CSA increased in order to restore a new morphodynamic equilibrium. The old channels at the sides of the estuary were abandoned and a new pattern oriented towards the barrage mouth formed, hereby relocating tidal flats that were initially located here. The new channel pattern caused the braiding index to decrease to a value of 1 in the barrage mouth and decreased the summed width of channels on both sides of the barrage.

The eroded material from the channels was transported in seaward direction. The initial modelled estuary had been already ebb-dominated, partly by the inflow of river water from upstream and partly by the initial, deep morphology. The morphology in the lower estuary and middle estuary was deepened further by the placement of the modelled tidal barrages here. This caused the estuary to locally become even more ebb-dominated, reflected by the a/h (decrease) and Vs/Vc (increase) ratios. The eroded material from the channels was not completely lost to the model sea, but instead was partly deposited on the tidal flats by tidal action. The result was an increase of area within the intertidal zone (based on offshore low- and high-water lines).

This thesis could contribute to the understanding of the effects of tidal barrage placement (modelled in the simplest way possible) on estuarine hydro- and morphodynamics. Up to this day, many of the effects of barrage placement on estuarine morphodynamics have not been studied thoroughly and a lot remains unknown. This hampers the implementation of more tidal energy plants like the La Rance tidal power plant, which has acted as a source of renewable energy for over 50 years. It is important to study the effects of tidal barrage on estuarine morphodynamics as this is coupled to estuarine ecology. The estuarine ecology is considered valuable and a lot of the potential sites for tidal range energy extraction are protected in projects like Natura2000.

References

Andre, H. (1978). Ten years of experience at the “La Rance” tidal power plant. Ocean Management, 4(2-4), 165-178.

Aubrey, D. G. (1986). Hydrodynamic controls on sediment transport in well-mixed bays and estuaries. Physics of shallow estuaries and bays, 16, 245-258.

Aubrey, A., & Elliott, M. (2006). The use of environmental integrative indicators to assess seabed disturbance in estuaries and coasts: application to the Humber Estuary, UK. *Marine Pollution Bulletin*, *53*(1-4), 175-185.

Bae, Y. H., Kim, K. O., & Choi, B. H. (2010). Lake Sihwa tidal power plant project. *Ocean Engineering*, *37*(5-6), 454-463.

Bodewes, B. (2015). Numerical modelling of the geologically reconstructed Oer-IJ estuary (Master's thesis).

Boon, J. D., & Byrne, R. J. (1981). On basin hypsometry and the morphodynamic response of coastal inlet systems. Marine Geology, 40(1-2), 27-48.

Burrows, R II., Walkington, I., Yates, N., Hedges, T., Chen, D., Li, M., ... & Prandle, D. (2009). Tapping the tidal power potential of the Eastern Irish Sea. Joule Project JIRP106/03, University of Liverpool and Proudman Oceanographic Laboratory, NERC.

Burrows, R I., Walkington, I. A., Yates, N. C., Hedges, T. S., Wolf, J., & Holt, J. (2009). The tidal range energy potential of the West Coast of the United Kingdom. Applied Ocean Research, 31(4), 229-238.

Charlier, R. H. (2007). Forty candles for the Rance River TPP tides provide renewable and sustainable power generation. Renewable and Sustainable Energy Reviews, 11(9), 2032-2057.

Cooper, N., Bailey, M., Mooyaart, L., Lansen, J., Jonkman, B., Van Haselen, C., & Royal Haskoning Nederland, R. (2009). Tidal Energy. Lessons Learnt from the United Kingdom and Opportunities for the Netherlands.

Dalrymple, R. W., Zaitlin, B. A., & Boyd, R. (1992). Estuarine facies models; conceptual basis and stratigraphic implications. Journal of Sedimentary Research, 62(6), 1130-1146.

De Haas, T., Pierik, H. J., Van der Spek, A. J. F., Cohen, K. M., Van Maanen, B., & Kleinhans, M. G. (2018). Holocene evolution of tidal systems in The Netherlands: Effects of rivers, coastal boundary conditions, eco-engineering species, inherited relief and human interference. Earth-Science Reviews, 177, 139-163.

Dronkers, J. (1986). Tidal asymmetry and estuarine morphology. Netherlands Journal of Sea Research, 20(2-3), 117-131.

Dronkers, J. (1998). Morphodynamics of the Dutch delta. Physics of Estuaries and Coastal Seas, 297-304.

de Laleu, V. (2009). La Rance Tidal Power Plant-40 Years Operational Feedback. *EDF, Liverpool*.

Falconer, R. A., Xia, J., Lin, B., & Ahmadian, R. (2009). The Severn Barrage and other tidal energy options: Hydrodynamic and power output modeling. Science in China Series E: Technological Sciences, 52(11), 3413-3424.

Friedrichs, C. T., & Aubrey, D. G. (1994). Tidal propagation in strongly convergent channels. *Journal of Geophysical Research: Oceans*, *99*(C2), 3321-3336.

Friedrichs, C. T., & Aubrey, D. G. (1988). Non-linear tidal distortion in shallow well-mixed estuaries: a synthesis. Estuarine, Coastal and Shelf Science, 27(5), 521-545.

Friedrichs, C. T. (2010). Barotropic tides in channelized estuaries. Contemporary issues in estuarine physics, 27-61.

Friedrichs, C. T. (2011). Tidal flat morphodynamics: a synthesis.

Garnier, R., Calvete, D., Falqués, A., & Caballeria, M. (2006). Generation and nonlinear evolution of shore-oblique/transverse sand bars. *Journal of Fluid Mechanics*, *567*, 327-360.

Gordon Jr, D. C. (1994). Intertidal ecology and potential power impacts, Bay of Fundy, Canada. Biological Journal of the Linnean Society, 51(1-2), 17-23.

Haverson, D., Bacon, J., Smith, H. C., Venugopal, V., & Xiao, Q. (2017). Cumulative impact assessment of tidal stream energy extraction in the Irish Sea. Ocean Engineering, 137, 417-428.

Hibma, A., Wang, Z. B., Stive, M. J. F., & De Vriend, H. J. (2008). Modelling impact of dredging and dumping in ebb-flood channel systems. Transactions of Tianjin University, 14(4), 271-281.

Hooper, T., & Austen, M. (2013). Tidal barrages in the UK: Ecological and social impacts, potential mitigation, and tools to support barrage planning. Renewable and Sustainable Energy Reviews, 23, 289-298.

Hume, T. M., & Herdendorf, C. E. (1988). A geomorphic classification of estuaries and its application to coastal resource management—a New Zealand example. Ocean and Shoreline Management, 11(3), 249-274.

Ibàñez, C., Prat, N., & Canicio, A. (1996). Changes in the hydrology and sediment transport produced by large dams on the lower Ebro river and its estuary. Regulated Rivers: Research & Management, 12(1), 51-62.

de Jonge, V. N., Schuttelaars, H. M., van Beusekom, J. E., Talke, S. A., & de Swart, H. E. (2014). The influence of channel deepening on estuarine turbidity levels and dynamics, as exemplified by the Ems estuary. Estuarine, Coastal and Shelf Science, 139, 46-59.

Kleinhans, M. G., Van Scheltinga, R. T., Van Der Vegt, M., & Markies, H. (2015). Turning the tide: Growth and dynamics of a tidal basin and inlet in experiments. Journal of Geophysical Research: Earth Surface, 120(1), 95-119.

Kleinhans, M. G., Van Der Vegt, M., Leuven, J., Braat, L., Markies, H., Simmelink, A., ... & Van Maarseveen, M. (2017). Turning the tide: comparison of tidal flow by periodic sea level fluctuation and by periodic bed tilting in scaled landscape experiments of estuaries. Earth Surface Dynamics, 5(4), 731-756.

Lanzoni, S., & Seminara, G. (1998). On tide propagation in convergent estuaries. Journal of Geophysical Research: Oceans, 103(C13), 30793-30812.

LeBlond, P. H. (1978). On tidal propagation in shallow rivers. Journal of Geophysical Research: Oceans, 83(C9), 4717-4721.

Leuven, J. R. F. W., Kleinhans, M. G., Weisscher, S. A. H., & Van der Vegt, M. (2016). Tidal sand bar dimensions and shapes in estuaries. Earth-science reviews, 161, 204-223.

Leuven, J. R. F. W., De Haas, T., Braat, L., & Kleinhans, M. G. (2018a). Topographic forcing of tidal sandbar patterns for irregular estuary planforms. Earth Surface Processes and Landforms, 43(1), 172-186.

Leuven, J. R., Verhoeve, S. L., Van Dijk, W. M., Selaković, S., & Kleinhans, M. G. (2018c). Empirical assessment tool for bathymetry, flow velocity and salinity in estuaries based on tidal amplitude and remotely-sensed imagery. *Remote Sensing*, *10*(12), 1915.

Leuven, J. R., Pierik, H. J., van der Vegt, M., Bouma, T. J., & Kleinhans, M. G. (2019). Sea-level-rise-induced threats depend on the size of tide-influenced estuaries worldwide. Nature Climate Change, 9(12), 986-992.

Lesser et al., 2004 G.R. Lesser, J.A. Roelvink, J.A.T.M. van Kester, G.S. Stelling Development and validation of a three-dimensional morphological model Coastal Engineering, 51 (8–9) (2004), pp. 883-915 (October)

Martin-Short, R., Hill, J., Kramer, S. C., Avdis, A., Allison, P. A., & Piggott, M. D. (2015). Tidal resource extraction in the Pentland Firth, UK: Potential impacts on flow regime and sediment transport in the Inner Sound of Stroma. Renewable Energy, 76, 596-607.

Nnafie, A., De Swart, H. E., Calvete, D., & Garnier, R. (2014). Modeling the response of shoreface-connected sand ridges to sand extraction on an inner shelf. Ocean dynamics, 64(5), 723-740.

Nnafie, A., Van Oyen, T., De Maerschalck, B., van der Vegt, M., & Wegen, M. V. D. (2018). Estuarine channel evolution in response to closure of secondary basins: An observational and morphodynamic modeling study of the Western Scheldt Estuary. *Journal of Geophysical Research: Earth Surface*, *123*(1), 167-186.

Neill, S. P., Litt, E. J., Couch, S. J., & Davies, A. G. (2009). The impact of tidal stream turbines on large-scale sediment dynamics. Renewable Energy, 34(12), 2803-2812.

Ranasinghe, R., Swinkels, C., Luijendijk, A., Roelvink, D., Bosboom, J., Stive, M., & Walstra, D. (2011). Morphodynamic upscaling with the MORFAC approach: Dependencies and sensitivities. *Coastal engineering*, *58*(8), 806-811.

Roelvink, J. A., & Walstra, D. J. (2004). Keeping it simple by using complex models. *Advances in Hydro-science and Engineering*, *6*, 1-11.

Roelvink, J. A. (2006). Coastal morphodynamic evolution techniques. Coastal engineering, 53(2-3), 277-287

Retiere, C. (1994). Tidal power and the aquatic environment of La Rance. *Biological Journal of the Linnean Society*, *51*(1-2), 25-36.

Pethick, J. S. (1984). *An introduction to coastal geomorphology*. Dept. of Geography, Univ. of Hull.

Prandle, D. (1984). Simple theory for designing tidal power schemes. Advances in water resources, 7(1), 21-27.

Pye, K., & Blott, S. J. (2014). The geomorphology of UK estuaries: the role of geological controls, antecedent conditions and human activities. Estuarine, Coastal and Shelf Science, 150, 196-214.

Savenije, H. H. (2015). Prediction in ungauged estuaries: An integrated theory. Water Resources Research, 51(4), 2464-2476.

Schuttelaars, H. M., & De Swart, H. E. (1999). Initial formation of channels and shoals in a short tidal embayment. Journal of fluid mechanics, 386, 15-42.

Speer, P. E., & Aubrey, D. G. (1985). A study of non-linear tidal propagation in shallow inlet/estuarine systems Part II: Theory. Estuarine, Coastal and Shelf Science, 21(2), 207-224.

Stevens, C. L., Smith, M. J., Grant, B., Stewart, C. L., & Divett, T. (2012). Tidal energy resource complexity in a large strait: The Karori Rip, Cook Strait. Continental Shelf Research, 33, 100-109.

Townend, I. (2005). An examination of empirical stability relationships for UK estuaries. Journal of Coastal Research, 1042-1053.

Turlings, L. G., Nieuwkamer, R. L. J., & Witteveen en Bos, D. (2009). Outline of Grevelingen for water and tide; Verkenning Grevelingen water en getij.

Uncles, R. J. (1981). A note on tidal asymmetry in the Severn estuary. Estuarine, Coastal and Shelf Science, 13(4), 419-432.

van Maanen, B., Coco, G., & Bryan, K. R. (2013). Modelling the effects of tidal range and initial bathymetry on the morphological evolution of tidal embayments. Geomorphology, 191, 23-34.

Veríssimo, H., Bremner, J., Garcia, C., Patrício, J., van der Linden, P., & Marques, J. C. (2012). Assessment of the subtidal macrobenthic community functioning of a temperate estuary following environmental restoration. Ecological Indicators, 23, 312-322.

Wolf, J., Walkington, I. A., Holt, J., & Burrows, R. (2009). Environmental impacts of tidal power schemes. In Proceedings of the Institution of Civil Engineers-Maritime Engineering (Vol. 162, No. 4, pp. 165-177). Thomas Telford Publishing.

Wang, Z. B. (2010). Morfologische effecten van een getijdecentrale in de Brouwersdam. Delft.

Xia, J., Falconer, R. A., & Lin, B. (2010). Impact of different tidal renewable energy projects on the hydrodynamic processes in the Severn Estuary, UK. Ocean Modelling, 32(1-2), 86-104.

Appendices

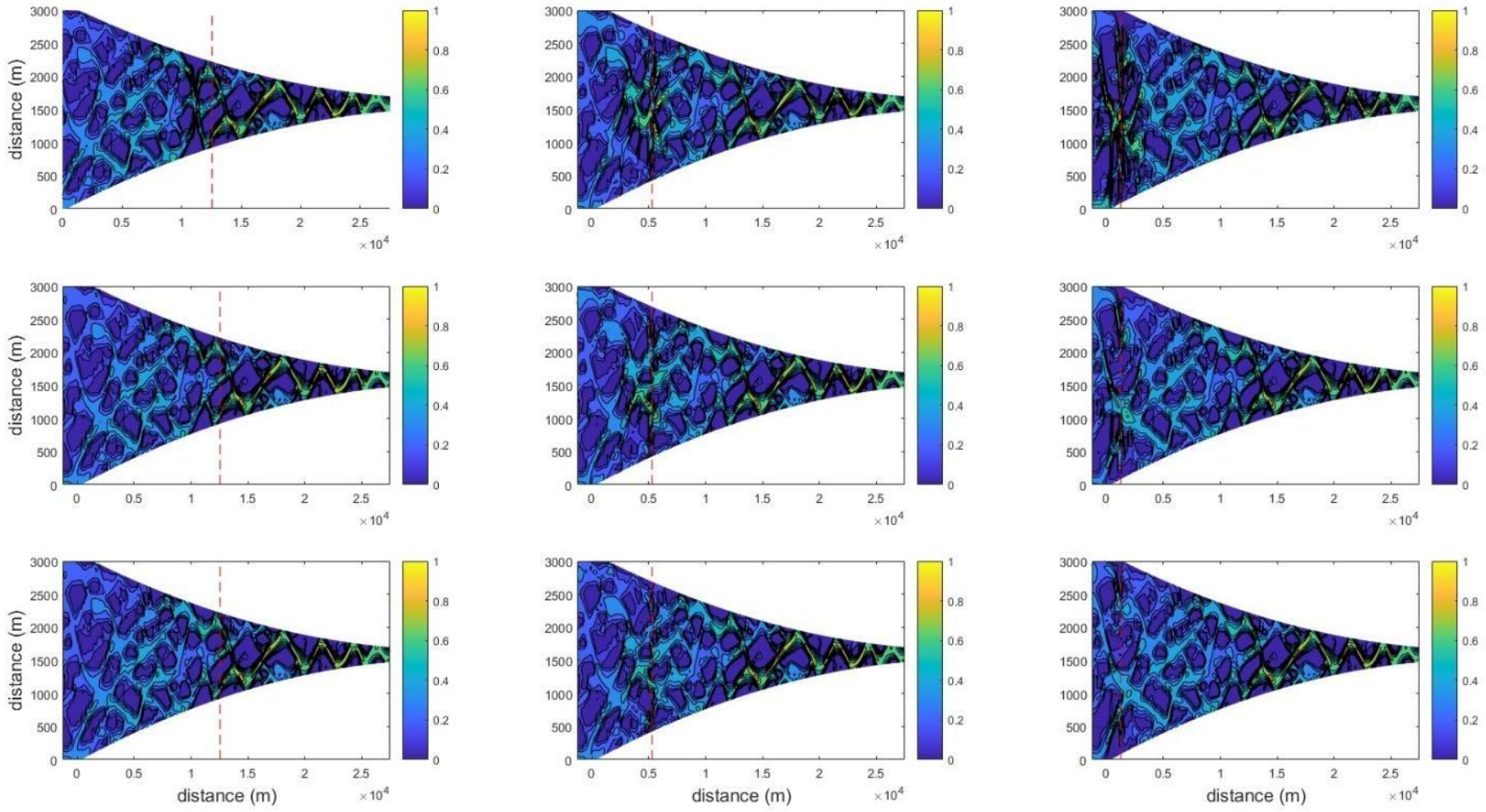

Appendix A: Flow velocity distribution throughout modelled estuaries. Top row =Cls-75-50, Cls-75-25, Cls-75-10 (from left to right; Second row: Cls-50-50, Cls-50-25, Cls-50-10; Third row: Cls-25-50, Cls-25-25, Cls-25-10

Run Name	Width reduction	Position TD	Tidal constituents	Bathymetry	Morfac	Max depth inlet (m)	Non-ero layer length (m)
Cls_0_0_Ndep2	-	-	M2	Ndep2	400	-	-
Cls_75_50	75%	N=290	M2	Ndep2	400	-	-
Cls_50_50	50%	N=290	M2	Ndep2	400	-	-
Cls_25_50	25%	N=290	M2	Ndep2	400	-	-
Cls_75_25	75%	N=160	M2	Ndep2	400	-	-
Cls_50_25	50%	N=160	M2	Ndep2	400	-	-
Cls_25_25	25%	N=160	M2	Ndep2	400	-	-
Cls_75_10	75%	N=86	M2	Ndep2	400	-	-
Cls_50_10	50%	N=86	M2	Ndep2	400	-	-
Cls_25_10	25%	N=86	M2	Ndep2	400	-	-
Cls_75_25_gat(5)	75%	N=160	M2	Ndep2	400	7	0
Morfac100_gat(5)_4months	75%	N=160	M2	Ndep2	100	7	0
Morfac100_gat(5)_4months	75%	N=160	M2	Ndep2	100	7	0
Morfac100_cls_50_10_gat(5)	50%	N=86	M2	Ndep2	100	7	0
max7_Cls_75_25_sed(6)	75%	N=160	M2	Ndep2	400	7	171
max7_Cls_75_25_Mor100_4m	75%	N=160	M2	Ndep2	100	7	171
max7_Cls_75_25(7)	75%	N=160	M2	Ndep2	400	7	171
max8_cls_75_10	75%	N=86	M2	Ndep2	400	8	175
max7_Cls_75_50	75%	N=290	M2	Ndep2	400	7	170
max7_Cls_75_25_long	75%	N=160	M2	Ndep2	400	7	339
max7_Cls_75_25_longer	75%	N=160	M2	Ndep2	400	7	506
SN_Cls_75_25	75%	N=160	O1, M2, M4	SN-equilibrium	400	-	-
SN_Cls_0_0	-	-	O1, M2, M4	SN-equilibrium	400	-	-
SN_max7_Cls_75_25	75%		O1, M2, M4	SN-equilibrium	400	7	171

Appendix B: More complete table of model runs. Most of them used in this report. Here the actual names of the model runs are used, which differ from some of the names used in the report.

Appendix C: Evolution of bathymetry in run Cls-75-25 for all 9 morphology outputs.

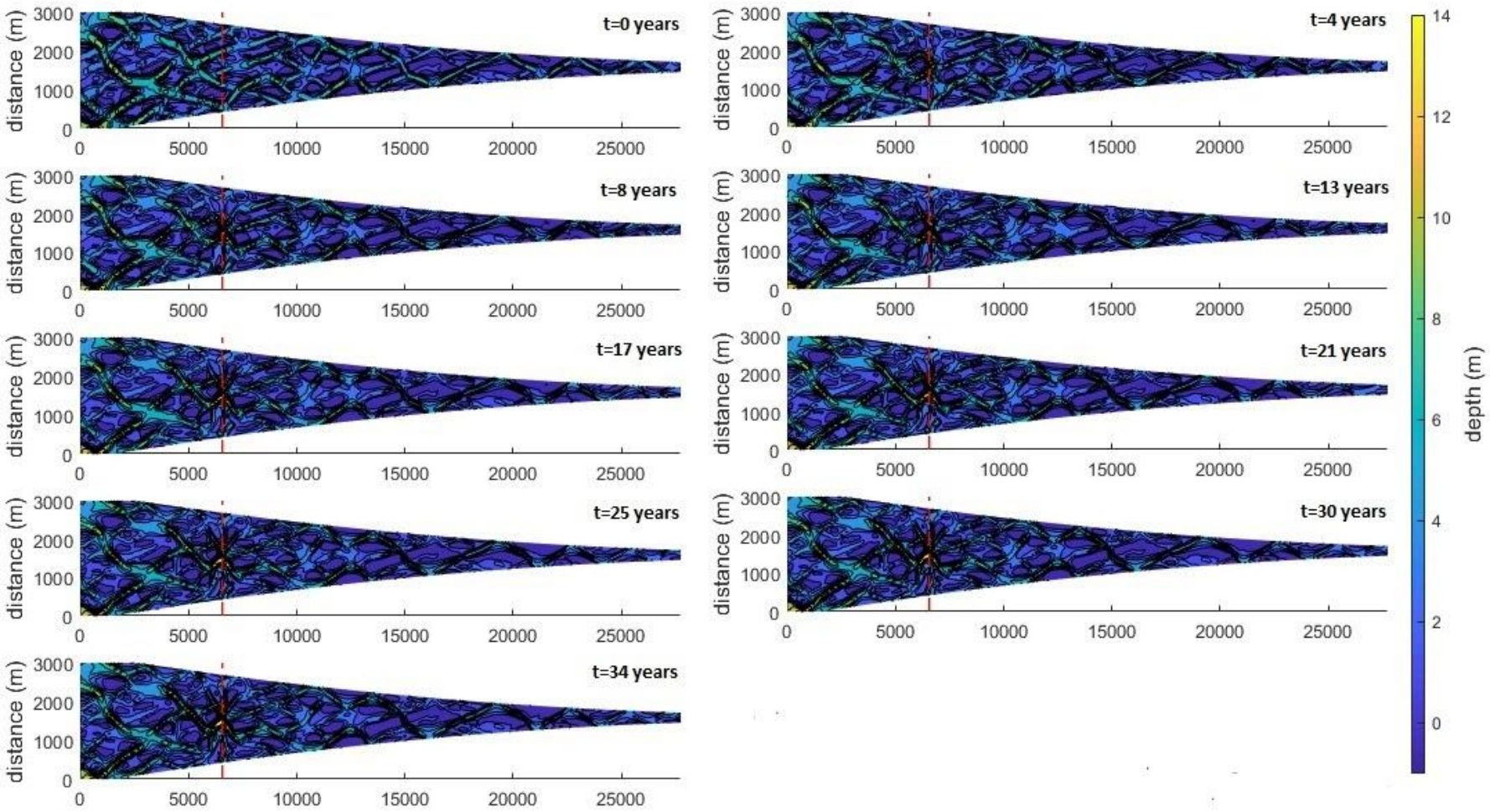

Appendix D: (on the next page) Overview of equilibrium bathymetry with thin dam positions indicated by red, dashed lines

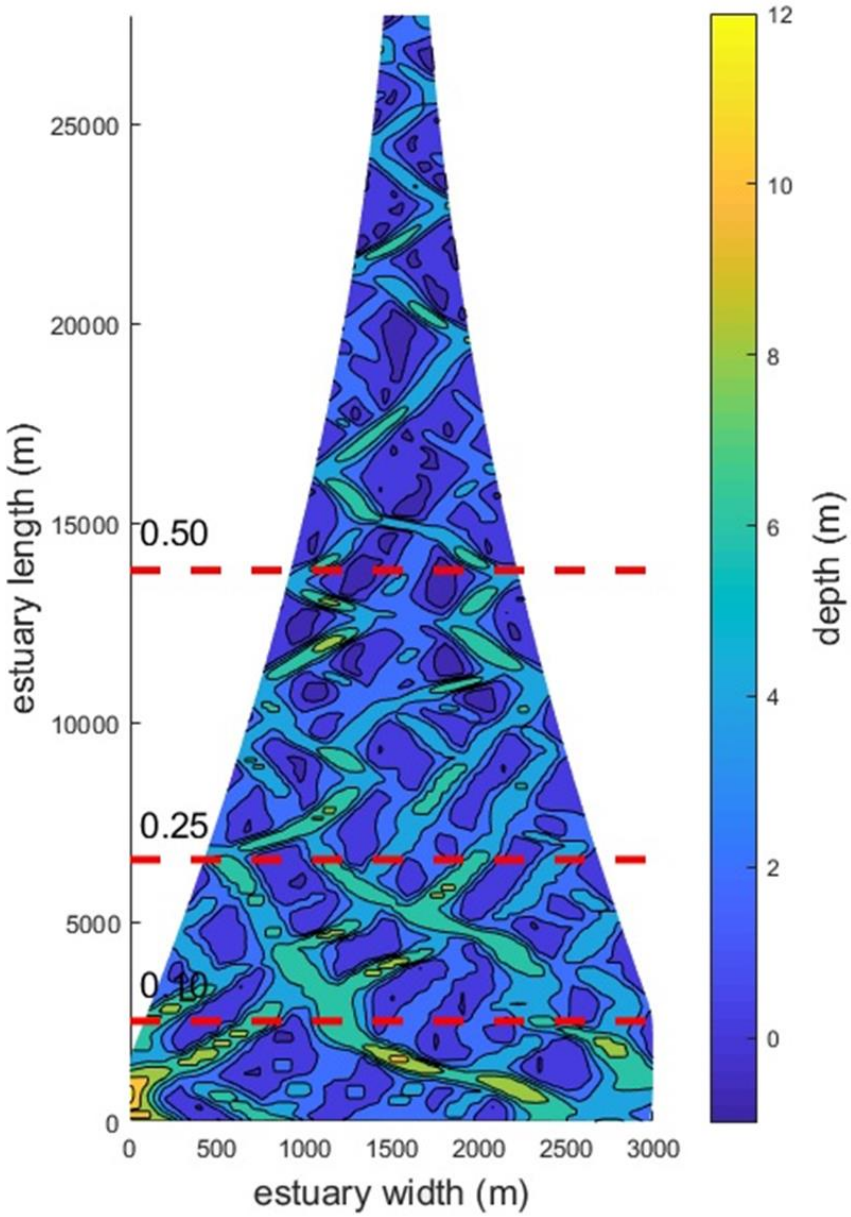
25000
20000
15000
10000
5000
0
estuary length (m)
0.50
0.25
0.10
0
500
1000
1500
2000
2500
3000
estuary width (m)
12
10
8
6
4
2
0
depth (m)

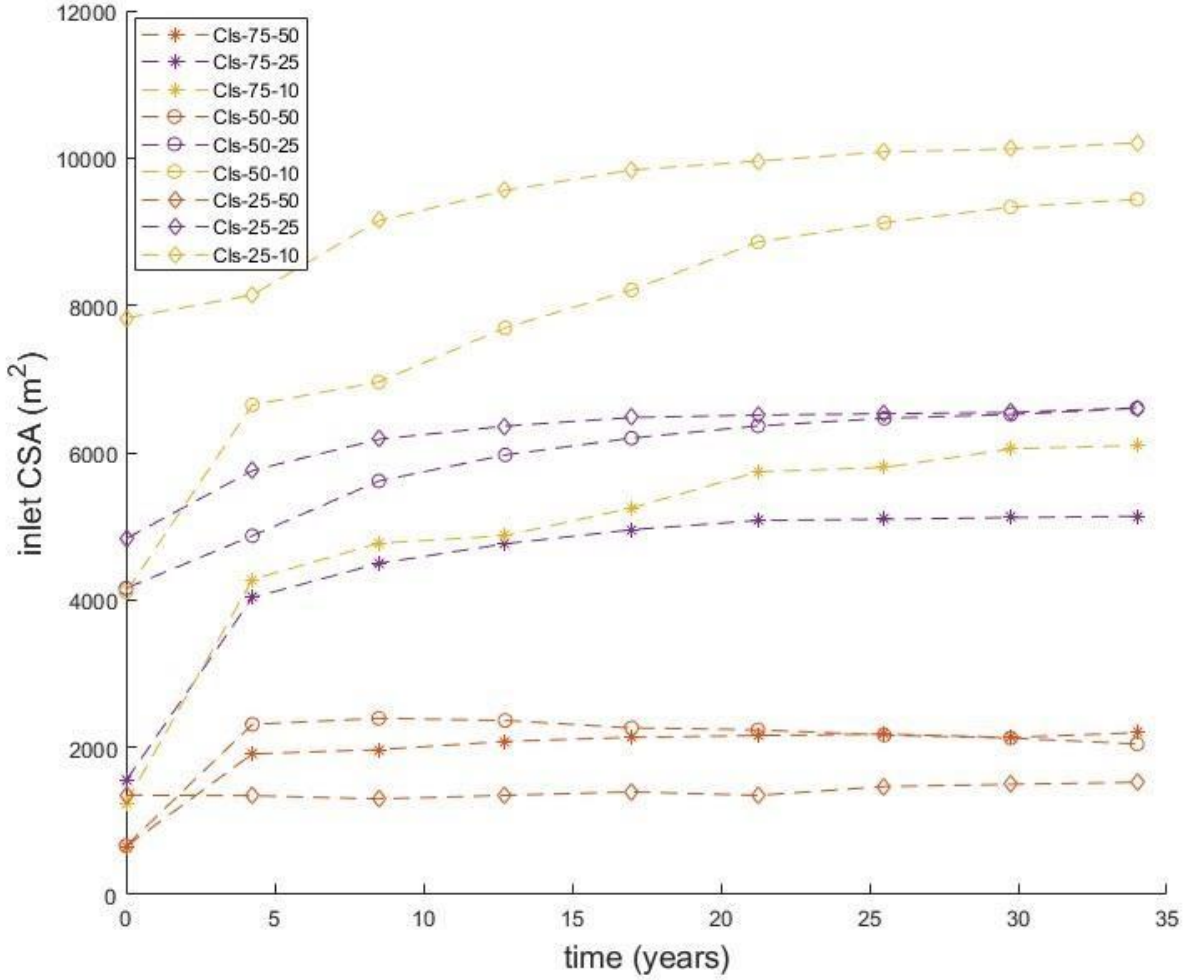

Appendix E: Evolution of the mouth cross-sectional area (CSA) over time for 9 Cls-runs.

Appendix F: Evolution of the mouth cross-sectional area (CSA) over time for 9 Cls-runs.

Parameter	Chézy	Morfac	H. timestep	M. timestep	Grainsize	Alphabn	Alphabs
Value	65	400	12	4.24	200	10	1
Unit	m0.5/s	-	min	year	µm	-	-